THE SPECTRA OF GALACTIC AND EXTRAGALACTIC RADIO SOURCES

Thesis by

Kenneth Irwin Kellermann

In Partial Fulfillment of the Requirements

For the Degree of

Doctor of Philosophy

California Institute of Technology

Pasadena, California

1963

ACKNOWLEDGMENTS

I would like to thank G. Stanley, research advisor during the course of this work and director of the Owens Valley Radio Observatory, for making available the large amount of observing time necessary to complete this project.

Thanks are also due to G. Seielstad, B. Clark, and D. Minalas who assisted with the observational program; to T. Matthews and M. Schmidt for providing unpublished material; and to the many people who contributed to the design, construction, and maintenance of the equipment at the Owens Valley Radio Observatory.

Some of the flux densities used to compile the spectra are based on unpublished observations by a number of workers at the Universities of Cambridge and Manchester. I am indebted to R. Long and R. Conway for making these results available.

Many stimulating discussions were held with G. Stanley, T. Matthews, R. Read, and J. Greenstein and I am grateful to them for their interest.

The research in radio astronomy at the California Institute of Technology is supported under the United States Office of Naval Research contract Nonr 220(19).

ABSTRACT

Observations have been made of the flux density of a number of discrete radio sources at 475, 710, 958, 1420, 2841, and 3200 Mc, using the two-element interferometer of the California Institute of Technology Radio Observatory. These have been combined with similar measurements at other frequencies made by different observers, to determine the spectral distribution for 242 sources where data is available over a wide range of frequencies.

It is shown that the spectra of most sources can be closely approximated by a simple power law of the form $S_f \propto f^{\alpha}$, at least between 38 and 1420 Mc. For these sources, the distribution of spectral indices is sharply peaked about a mean value of -0.77 with 50 per cent of the sources having an index between -0.70 and -0.85. No sources were found with an index steeper than -1.23. In some cases, the spectral index is a function of frequency over the observed range from 38 to 3200 Mc. For these sources, which generally have a high surface brightness, the typical change in spectral index is about 0.5 in the sense that the spectrum is flatter at longer wavelength.

The observed spectral distributions are interpreted in terms of synchrotron radiation and it is postulated that the bright sources having a curved spectrum are relatively young and rapidly evolving toward a power law spectrum.

TABLE OF CONTENTS

I. INTRODUCTION

It is now generally accepted that the emission of radio frequency energy in non-thermal radio sources is primarily due to synchrotron radiation from ultrarelativistic electrons gyrating in weak magnetic fields. As shown in Chapter V the frequency dependence of synchrotron radiation depends only on the energy distribution of these electrons. Thus, the observed spectrum provides a powerful tool for the investigation of the distribution of particle energies within a source. Since the spectral dependence of the radiation is closely related to the internal conditions in a source, it is expected that a knowledge of their spectra will contribute to the understanding of their origin and evolution.

Variations in the spectra of different sources can be used to classify the sources and possibly to relate these differences to other observed properties of the sources. If, in addition, the distance to the source is known from an optical identification, the radio spectrum can be used to obtain an estimate of the total energy involved in the emission process.

The earliest investigation of the spectra of radio sources was by Stanley and Slee in 1950 (1). Their observations, although not of the highest accuracy, clearly showed that for at least three of the four sources investigated, the observed spectra did not agree well with that expected from thermal radiation.

Whitfield (2)(3) in 1957 used observations made at Cambridge at 38, 81.5, and 159 Mc along with previously published data, to determine the spectra of a number of sources. He found that the average spectral index of the galactic sources was noticeably flatter than that of the nongalactic ones. He also showed that the spectrum of Cygnus A did not follow a simple power law, and that the spectral index became steeper at high frequencies.

The first extensive set of observations at decimeter wavelengths was by Harris and Roberts (4) at Caltech. By comparing their 960 Mc observations with those of Cambridge at 159 Mc and 178 Mc, they were able to show that the spectral indices of the galactic sources showed a much wider dispersion than those of the extragalactic sources. Harris has attempted to interpret the differences in the spectra of the galactic sources in terms of their evolution (5).

The present work, based on observations over a wide range of frequencies, provides for the first time fairly detailed spectra for a large number of sources.

Most of the sources reported here are at high galactic latitude and are believed to be of extragalactic origin. About fifty of these are identified with so-called "radio galaxies" whose output of radio energy ranges from 10 to 10^6 times that of our own Galaxy. There is now increasing evidence that the majority of the unidentified sources are likewise powerful radio emitters located at very great distances.

The new observational data comes from measurements by the author, of the flux densities of several hundred sources at 475, 710, 958, 1420, 2841, and 3200 Mc using the two-element interferometer of the Owens Valley Radio Observatory. These have been combined with recent measurements at lower frequencies made at the University of Cambridge and at the University of Manchester, and with previously published data to determine the spectra of 242 sources. Systematic errors arising from the various techniques used by the different observers have been minimized by using a uniform procedure to correct for errors introduced by instrumental effects such as confusion, resolution, and uncertain source positions.

The Caltech results between 475 Mc and 2840 Mc are believed to form an especially self-consistent set of data as the same observing and reduction techniques were used at each frequency. The equipment used for these observations is described in Chapter II along with an outline of the observing and reduction procedure employed. The results of the flux density measurements are given in Chapter III, and the spectra derived from these data are presented and discussed in Chapter IV. In Chapter V the observational results are discussed in terms of synchrotron radiation.

II. THE OBSERVATIONS

Given a point source of radiation, the power accepted by an antenna in a bandwidth $\Delta\nu$ is given by

$$p = \beta S_\nu A_{eff} \Delta\nu \qquad (2.1)$$

where S is the flux density of the source, A_{eff} is the effective area of the antenna, and the factor β depends on the polarization of the incident radiation. For a plane polarized antenna, β is equal to one-half if the radiation is random or circularly polarized. Otherwise, it depends on the direction and degree of polarization.

If we replace the antenna with a matched resistor at a temperature ΔT, the power available is

$$p = k \Delta\nu \Delta T \qquad (2.2)$$

where k is Boltzman's constant and ΔT is termed the antenna temperature. Equating equations 2.1 and 2.2 we find*

$$S_\nu = \frac{2}{A_{eff}} \Delta T \quad . \qquad (2.3)$$

Thus, to obtain an absolute measurement of flux density, two quantities must be determined: the effective area, A_{eff} and the change in antenna temperature, ΔT when the antenna is pointed toward a source.

The accurate measurement of these quantities requires a knowledge of the gain of the antenna and the

---

*We shall assume that $\beta = 1/2$.

sensitivity of the receiver, both of which are difficult to determine in practice. However, if the gain of the antenna can be assumed to remain constant, then relative intensities can be determined simply be measuring relative changes in the antenna temperature. The present observations constitute such a set of relative measurements. At each frequency these relative measurements have been placed on an "absolute" basis by making use of published flux densities for the source Cass A.

2.1 Interferometer Observations

With the exception of 3200 Mc, all of the observations reported here have been carried out using the two 90-foot paraboloids at the Owens Valley Radio Observatory as an interferometer.

Each antenna was fed by a rectangular horn at 958 and 1420 Mc, and by a dipole in front of a 120^{o} corner reflector at 475 and 710 Mc. These feeds gave an illumination at the edge of the dish that was about 10 per cent of that at the center, resulting in a nearly circular beam pattern. The nearest side lobe was at least 20 db below the main beam. At 2840 Mc, a more heavily tapered feed was used to minimize the effects of surface irregularities near the outer part of the dish. In each case the feed was positioned so that the antenna was sensitive to radiation whose electric vector was in position angle zero.

At the lower frequencies, the efficiency of the dish

Table I

Frequency (Mc.)	Number of Sources Observed	Time of Observation	Primary Beam Width	Interferometer Spacing	Approximate System Noise Temperature	RMS Noise Uncertainty in Single 10 Minute Observation*	RMS Confusion Level*
475	78	Jan. 1962	95'	100λ	600°	.4+	.9
710	126	Dec. 1961	72'	150λ	300°	.1	.4
958	229	Aug. 1961 March 1962	48'	100λ	300°	.1	.25
1420.4	207	Sept. 1961 Feb. 1962	36'	150λ	350°	.13	.15
2841	67	April 1962 Nov. 1962	18'	300λ	600°	.25	.05
3200	35	July-Aug. 1961	16'	Pencil Beam	1200°	±2.0	.07

* Units of 10^{-26} Watts/meter^2/cps.

±Due in part to short term gain instabilities.

+Due in part to baseline fluctuations.

was between 50 and 60 per cent, while at 2840 Mc it fell to about 35 per cent.

A crystal mixer and a 10 Mc i.f. preamplifier were mounted at the focus of each antenna. The excess noise temperature at 710, 958, and 1420 Mc was roughly equal to the antenna temperature of the source Cass A (see Table I). At 475 Mc the sensitivity was considerably poorer as the mixer used at this frequency was the one designed for use at 958 Mc.

At 475 and 710 Mc the power from the local oscillator, located in the laboratory, was sent directly to each antenna through coaxial cable. At the higher frequencies, this master oscillator was used to provide a reference signal to which separate klystron oscillators located at the focus of each antenna could be locked. This phase lock system has been described in detail by Read (6).

Since no image rejection was used, the system is sensitive to two bands of frequencies, each about 4 Mc wide and spaced 10 Mc on either side of the local oscillator frequency. The flux densities quoted here are thus averages over a 20 Mc range and the specified frequency refers to that of the local oscillator. The i.f. signals from the two antennas were combined in a continuous multiplier followed by a 10 or 20 second output time constant and pen recorder.

The form of the output function and its relation to the geometry of the interferometer and the receiver

parameters has been discussed by Read (7) and by Moffet (8). For our purposes, it is sufficient to note that the interferometer output function is a quasi-sinusoid whose amplitude is nearly proportional to the antenna temperature of a "point" source. The exact relation between flux density and recorder deflection for an arbitrary detector law is given in Appendix I. The response of an interferometer to a source of finite angular extent has been given by Moffet (8) and others.

At 958 and 1420 Mc most of the observations were made at night to avoid any effects of solar radiation. These observations were carried out in two observing periods spaced about six months apart. Due to the high mountains surrounding the Owens Valley Radio Observatory, which lengthen the period each day when the sun is below the horizon, there was a considerable overlap period which could be observed in "darkness" both times. Sources crossing the meridian during this period, as well as a number of intense sources observed in the daylight were used to tie together the two sets of observations.

At 475 and 710 Mc only a single series of observations was made in December and January when the sun is above the horizon for only about eight hours each day. Some deterioration in the quality of the records was noticed during this time. The records of a few sources located close to the sun showed evidence of interference and these were discarded.

Most of the results at 2840 Mc are based on observations made by J. F. Bartlett for the purpose of deter-

mining brightness distributions. In a few cases of special interest, special observations were made by the author at an antenna spacing of 300 wavelengths.

The observing procedure at each frequency was to track the antennas at an assumed position of the source for about fifteen minutes near transit. The mean amplitude of the interference pattern was then determined by averaging the amplitude of from five to ten fringes, and was corrected for the attenuation of the output time constant. Each source was observed on a number of nights and the quoted flux density is based on the mean of all the observations. In all, about 2,500 individual observations were obtained.

Noise fluctuations

Under idealized operating conditions a two-element interferometer collects, on the average, twice as much signal power as a single element operating alone as a simple radiometer. In practice however, when used to measure accurate intensity ratios, the interferometer presents several distinct advantages that cannot be explained in terms of mere signal-to-noise ratio.

As the output of the interferometer is quasi-periodic, it is quite feasible to recognize the characteristic interference pattern even when the signal-to-noise ratio is of the order of unity. Furthermore, each interference fringe constitutes an independent measurement of the source strength, and it is thus possible to average a number of consecutive

fringes to obtain a measure of the source intensity. It should be noted that as the phase of the interference pattern can easily be estimated by inspection of the record, the procedure of averaging successive fringes is equivalent to coherently averaging a number of independent measurements.

In contrast, in the case of a simple radiometer, the response of the receiver to a source passing through the antenna beam consists of a single deflection which, for small signal-to-noise ratios, is often difficult to distinguish from random noise fluctuations. Moreover, the usual technique of taking "drift curves" requires that the majority of the observing time be spent in determining the zero level of the receiver.

In principle the fraction of time spent "on source" could be increased to one-half by alternately pointing the antenna toward and away from the source. However, this procedure is usually unsatisfactory due to the rapid change in the ground and background radiation caused by the motion of the antenna.

In addition, in order to improve the stability of a simple radiometer, it is the usual practice to compare the signal from the antenna with the noise from a "cold" load. Since this results in observing the source only half the time and noise all the time, we lose a factor of two in the theoretical signal-to-noise ratio.

Finally, we point out that, since the coherence of the radiation field depends on the angular extent of the

source of radiation, the interferometer will respond only to "point" sources and will be insensitive to gradients in the background or to extended sources of radiation. Furthermore, the use of a multiplying type of interferometer as is in use at the Owens Valley Radio Observatory eliminates the need for highly stable preamplifiers as the equipment only responds to signals that are correlated between both antennas (Appendix I). This also reduces the effect of varying ground radiation and external interference.

Confusion

The problem of confusion has been discussed by a number of authors (9), (10), (11). The following discussion is patterned after Mills and Slee (9), but is applied specifically to interferometers.

We let N(S) be the number of sources per steradian with flux density greater than S and Ω , the solid angle subtended by the antenna beam. If we assume that the sources are randomly distributed throughout the sky, the mean number of sources with flux density greater than S in the beam is $n(s) = N(S)\Omega$.

If the number flux relation is given by

$$N(S) = KS^{x} \quad , \qquad (2.4)$$

then the mean number of sources in the beam brighter than S is

$$n(s) = KS^{x}\Omega \quad , \qquad (2.5)$$

and the number between S and S+ds

$$dn(s) = -xKS^{x-1}\Omega \, dS \equiv \sigma^2 \quad . \tag{2.6}$$

As these dn sources add in random phase, the net contribution to the observed fringe amplitude is given by $\sigma_s = \sigma S$. Thus,

$$\sigma_s^2 = \sigma^2 S^2 = -xKS^{x+1}\Omega \, dS \quad . \tag{2.7}$$

To get the total contribution from all sources, we integrate overall values of S

$$\Delta S^2 = -xK\Omega \int_{S_{min}}^{S_{max}} s^{x+1} \, dS \quad ;$$

Therefore,

$$\Delta S = \left\{ - \frac{xK\Omega}{x+2} \right\}^{1/2} \left\{ S_{max}^{x+2} - S_{min}^{x+2} \right\}^{1/2} \quad . \tag{2.8}$$

As shown by Ryle (10), the output of an interferometer will be equal to the vector sum of the source under study and all the confusing sources in the beam. Thus, if ΔS is the sum of the confusing sources and S the flux of the source, the observed flux density is given by

$$S_{obs}^2 = S^2 + (\Delta S)^2 - 2S\Delta S \cos \phi \quad . \tag{2.9}$$

Then

$$S \simeq S_{obs} \left[1 + \left(\frac{\Delta S}{S} \right) \cos \phi - \frac{1}{2} \left(\frac{\Delta S}{S} \right)^2 + \left(\frac{\Delta S}{S} \right)^2 \cos^2 \phi \right] , \tag{2.10}$$

where ϕ is the phase difference between the two antennas.

The second term represents a random error whose r.m.s. amplitude is given by

$$\delta S = (\Delta S^2 \overline{\cos^2\phi})^{1/2} = \frac{1}{\sqrt{2}}\Delta S \quad . \qquad (2.11)$$

In addition, there is a small second order term, $\frac{1}{4}(\frac{\Delta S}{S})^2 S$, to correct for the systematic over estimation of the flux density for sources that are near the confusion limit.

If we make the reasonable assumption that there are no confusing sources in the beam stronger than the source under study, we can let $S_{max}=S$, and if $\frac{S_{min}}{S} \ll 1$ we can write equation 2.08 as

$$(\Delta S)^2 = - \frac{xK\Omega}{x+2} S^{x+2} \quad . \qquad (2.12)$$

If we define the fractional error

$$\gamma^2 = (\frac{\Delta S}{S})^2 = - \frac{xK\Omega}{x+2} S^x = - \frac{x\Omega}{x+2} N(S), \qquad (2.13)$$

then the number of sources per steradian such that the r.m.s. uncertainty in the measured flux density is less than γ is

$$N(S) = \gamma^2 (\frac{x+2}{-x}) \frac{1}{\Omega} \quad . \qquad (2.14)$$

We define the number of beamwidths per source, n_o, giving

$$\gamma^2 = N(S)\ \Omega\ (\frac{-x}{x+2}) = \frac{1}{n_o}(\frac{-x}{x+2}) = \frac{9}{n_o} \text{ for } x = -1.8 \qquad (2.15)$$

Thus we see that the often quoted level of reliability of $n_o=20$ gives an r.m.s. error of 40 per cent for the weaker

sources.

The numerical values of K,x,S_{max} and S_{min} are not well determined, and there is considerable disagreement among various workers as to the actual form of the number flux relation (12)(13). The most extensive work in this field has been done by Ryle and his colleagues at Cambridge. From their results at 178 Mc (14), expression 2.08 was used to determine the number flux relation at the various frequencies where observations have been made. These were then used to estimate the uncertainty due to confusion shown in Table 1.

Antenna pointing errors

Since all the observations were based on an assumed position of the source, any error in this position greater than about 5 per cent of the antenna beamwidth will result in a noticeable reduction in the observed fringe amplitude. Accurate positions for many sources were available from the work of Matthews (15) and Read (6) at Caltech, or Elsmore, Ryle, and Leslie (16) at Cambridge.

In a number of cases where new position information became available after the observations were completed, corrections were applied to the observed amplitudes. Rather large corrections were sometimes necessary where the positions in the original 3C catalogue (7) were incorrect by one or more interference fringes. The revised 3C catalogue of Bennet (18) was used to check the position of most of the

sources in the northern hemisphere, and the probability of any remaining lobe shift errors in these sources is small. Accurate positions of some sources in the southern hemisphere were kindly made available by Bolton, et al(19) and were used to correct the observed flux densities for those sources whose positions had not been measured at Caltech. The rather poor agreement between the original positions of Mills, Slee, and Hill (20)(21) and the newer positions suggests somewhat greater errors in the positions than estimated by the authors. Thus the flux densities for the southern sources for which there are no accurate positions may be considerably underestimated.

A similar reduction in the measured flux density may arise from an uncertainty of one to two minutes of arc in the pointing of the telescope. In a few cases the amplitude of a single record was found to be considerably less than on other records of the same source. This was undoubtedly due to an error on the part of the operator in setting the telescope, and such records were discarded.

Effect of finite bandwidth

As has been shown by Read (7), the amplitude of the interference pattern of a double sideband receiver of finite bandwidth is modulated by a function of the form

$$p \simeq q(\sin\theta)\cos\left(\frac{\omega_{if}}{c} D \sin\theta\right) \qquad (2.16)$$

where q is a function of the i.f. bandpass which changes

slowly with hour angle near transit, θ is the angle between the source and a plane normal to the two antennas, D is the separation of the two antennas, ω_{if} the effective i.f. frequency, and c the speed of light.

For a perfect east-west interferometer and for small values of θ (i.e. near transit)

$$\sin\theta \simeq \theta \simeq H\cos\delta \qquad (2.17)$$

where δ and H are the declination and hour angle of the source. Thus,

$$p \simeq q\left(H\cos\delta\right) \cos\left[\frac{\omega_{if}}{c} DH\cos\delta\right] \quad . \qquad (2.18)$$

The dominant factor of the interferometer function is well known from elementary theory to be of the form

$$F(\theta) = \cos\left[\frac{\omega_{lo}}{c} D \sin\theta\right] \qquad (2.19)$$

where ω_{lo} is the local oscillator frequency. Substituting equation 2.17 we have

$$F(H) = \cos\left[\frac{\omega_{lo}}{c} DH \cos\delta\right] \quad . \qquad (2.20)$$

Comparing equations 2.18 and 2.20, we see that both the primary interference pattern and the modulating function are almost periodic functions of the hour angle whose periods for a given antenna spacing are both proportional to Sec δ. The other factors in equation 2.28 vary slowly enough that

they can be ignored for small hour angles. Therefore, the "n^{th}" interference lobe from transit will always be reduced in amplitude by the same factor at all declinations.

While the necessary correction for the effect of the finite bandwidth can in principle be calculated from a knowledge of the receiver parameters and the geometry of the interferometer, we have instead measured the modulating function directly on a strong source at each frequency.

For most of the sources, a fixed number of fringes centered on the zero order fringe were observed. Since the correction factor depends only on the fringe number, no corrections are needed in these relative amplitudes. In a number of cases where the observing schedule required that the observation be made a few minutes off transit, the observed amplitudes were corrected. In only a few instances did this correction amount to more than 1 per cent.

In those cases where the observation was centered more than about 10 minutes from transit, additional delay was placed in the proper arm of the interferometer to bring the central fringe to the middle of the record. These observations are subject to a somewhat greater uncertainty since the delay used could only be changed in discrete steps of 3×10^{-9} seconds corresponding to 7 minutes of time at an antenna spacing of 100 feet.

Resolution

The output of the interferometer is proportional to

the Fourier spatial frequency component of the brightness distribution corresponding to the separation of the antenna elements (8). Therefore, a source whose angular extent in the sky is not negligible when compared to the interferometer fringe spacing, will thus be recorded with less amplitude than a point source of equal flux density. To eliminate so far as possible the effect of resolution, all observations were made with the closest practical antenna spacing. However, corrections are still necessary when the size of the source is greater than a few minutes of arc.

The angular size of many of the sources studied here has been investigated by Moffet and Maltby (8)(22). For these sources the present observations at 958 Mc were used to provide improved estimates of the behavior of the visibility function below 200λ. The visibility functions were then used to correct the observed amplitudes to zero antenna spacing, that is corresponding to the total intensity of the source. With the exception of 2840 Mc all the observations were made at an antenna spacing of 100λ or 150λ. Since the same source models were used at all frequencies, it is expected that partial resolution will have little effect on the measured relative flux densities of a given source at different frequencies.

Where detailed visibility functions were not available at 958 Mc, the recent investigations of angular size at Jodrell Bank (23), Cambridge (18), and Sydney (21) were used to determine the corrections for resolution. In the latter

two cases, the diameters quoted by the authors are based on measurements made with a single antenna spacing which, considering the known complex structure of the sources must be treated with caution.

As these measurements were not generally made at the same frequencies as the present set of observations, the question arises as to how much the above procedure is affected by changes in the angular structure of the sources with frequency. A comparison of the visibilities measured at 159 and 960 Mc by Moffet and Palmer (24) indicates that with few exceptions there is little evidence of any variation in the structure of the sources with frequency.

For most of the sources observed in the present program, the diameter was sufficiently small in comparison to the interferometer fringe spacing that corrections to the measured amplitude of more than a few per cent were necessary in only a small number of cases. Thus any slight dependence of the size on frequency that may exist is felt to have a negligible effect in making these corrections.

Over half the sources were essentially unresolved and no corrections were necessary.

Gain variations

While the use of an AGC in each i.f. channel eliminates the usual need for extremely great gain stability in the preamplifier, it has several drawbacks that must be considered. Since the effect of the AGC is to keep the noise power pre-

sented to the second detector constant, any variation in the noise coming from the preamplifier will cause a change in the gain of the system. Thus variations in the noise figure of the receiver will be reflected as a gain change. Furthermore, since the antenna temperature depends on the flux density of the source, the gain of the system will depend on the strength of the source being observed. With the exception of the few very strong sources, this change is less than a few per cent of the total system temperature; and for the majority of the sources observed here, the correction for the AGC gain reduction was only a few tenths of a per cent.

What is perhaps more serious however, is the change in the antenna temperature due to changes in the background temperature or ground radiation being picked up in the distant side lobes. The former is the most serious in the vicinity of the galactic center and the latter at very low southern declinations. Likewise, any low level interference that is picked up will cause a similar reduction in the gain.

For a few very strong sources where the antenna temperature is of the same order as the receiver noise temperature, the corrections become very large, and the uncertainties in the receiver noise figure did not allow this correction to be made with reasonable accuracy. Moreover, for these sources the effect of the non-linearity of the detector law becomes important as described in Appendix 1. Since these sources have been observed by a large number of workers over a wide range

of frequencies, they were not included in the present program of observations.

As there was no means of directly checking the gain of the system, a series of strong calibration sources was observed each night. Over most of an observing period the gain appeared to remain constant to within about 2 or 3 per cent. Variations of this order occurred within a few minutes and therefore the calibrators which are usually spaced several hours apart could not be used to remove this small uncertainty in the gain. The cause of this gain variation appears to be due to small changes in the noise figure of the receiver which are presumably caused by changes in the local oscillator power fed to the mixer. This effect was especially noticeable at 475 Mc where the local oscillator power was fed to the antenna through several hundred feet of coaxial cable. Due to the poor match between the line and the mixer, large standing waves were present on the line, and changes in the length due to large temperature changes (sometimes as much as 40°F within a few hours) thus caused variations in the crystal current by as much as a factor of two.

One disadvantage of this system over the usual method of using a noise source to calibrate the gain, is that any gain changes that occur at the same time each day will go unnoticed. Comparison of the relative intensities of the strong sources observed six months apart at 958 and 1420 Mc at different times of the day did not show any evidence for such systematic gain changes. However, when compared with

the 958 Mc data of Moffet (8) it was found that the intensity of most of the sources between about 3C 200 and 3C 300 were a few per cent lower than obtained by Moffet. One possible explanation of this effect is that low level i.f. interference was causing a gain reduction. The present observations of these sources were made near midnight in March when propagation at 10 Mc is extremely good. However, due to the small amplitude of the effect and the uncertainty in its origin, no changes were made in the observed values.

A similar effect was found in the 475 Mc data where it was found that the observed flux densities for the sources observed just after sunset were consistently high when compared to the flux density predicted from the spectrum derived from the observed fluxes at other frequencies. For these sources a single correction factor was applied to bring the final flux densities into better agreement with the observations at the other frequencies.

In general the uncertainty in the gain calibration at 475 Mc was considerably greater than at the other frequencies, being about 10 per cent at any given time. It is not clear whether this was due to the thermal effects discussed above or to variations in the ionospheric attenuation.

In this respect it is interesting to note that at 475 Mc, and to a lesser extent at 710 Mc, the noise level suddenly increased just after sunset and just before sunrise each day, making observations practically impossible. This

effect lasted for about an hour, but its duration and severity varied from day to day.

2.2 Pencil Beam Observations

The observations at 3200 Mc were made with a traveling wave-tube radiometer and a single 90-foot antenna. A ferrite circulator was used to switch the receiver between the main beam and a reference beam 1-1/2 degrees south of the main beam. The low noise traveling wave-tube amplifier at the focus of the antenna, after additional r.f. amplification, was followed by an r.f. detector, audio amplifier, and synchronous detector. A ten-second time constant was placed between the output of the radiometer and pen recorder.

The receiver had an excess noise temperature of about 1200 degrees K and a 350 Mc bandwidth.

At this frequency, the sensitivity was limited by short term gain fluctuations equivalent in amplitude to a source of a few flux units. The design and construction of the receiver were due to Dr. A. T. Moffet who also collaborated in the observations at this frequency.

At the beginning of the observing period, two days were spent in observing the four strong sources Cass A, Taurus A, Cygnus A, and Virgo A. The apparent position of each source was first measured to an accuracy of about 0.'5, and then the deflection of the source relative to the background was determined by alternately pointing the antenna toward and away from the source. By going back and forth

between two sources it was possible to obtain accurate relative intensities for these four sources.

The differences between the apparent positions of the source as measured above and the known positions were then used to determine the antenna pointing errors. These were plotted as a function of hour angle for each source and used to calibrate the pointing of the antenna for the subsequent observations.

The same four sources were constantly observed throughout the remainder of the observing period and their relative amplitudes were used to calibrate the sensitivity of the receiver. Each observation of a source consisted of taking several drift curves and for most of the sources this procedure was repeated on a number of days.

It was found that after the first few days of operation, the noise figure of the traveling wave-tube began to deteriorate. After ten days it had become so bad that it was necessary to terminate the observations. Because of the fairly rapid change in sensitivity with time, the gain calibration at any instant was only known to about 10 per cent and this constituted one of the main sources of error at this frequency.

Where necessary, the observed fluxes were corrected for the effect of resolution by the 16' antenna beam. This correction, in general, did not amount to more than a few per cent.

III. The Flux Densities

In order to determine the spectra of the sources, it is necessary to place the measured relative flux densities at each frequency on some absolute scale. Because of the well known difficulties in measuring absolute flux densities, it has become the practice to present spectra relative to some standard source, usually Cassiopeia A (2)(25)(26) as this source has the most reliably determined absolute spectrum.

However, even for relative spectra this procedure is unreliable for several reasons. First, the antenna temperature due to the brightest sources commonly used for calibration is often comparable with the system noise-temperature. The corresponding receiver non-linearity thus makes it difficult to obtain accurate measurements of the large ratios of the flux density of these sources to those of the majority of sources. Secondly, the angular size of these sources makes them unsuitable for calibration of flux density measurements made with an interferometer. Thirdly, it is now evident that the flux density of Cass A is decreasing at a rate of about 1 per cent per year (27)(28). The uncertainty in this rate of decrease makes it difficult to use these sources for the comparison of observations made more than a few years apart. Finally, by using only a single calibration source, random errors in the determination of its relative flux density at any one frequency will cause a systematic error in the relative flux density of the remaining sources.

The following procedure for obtaining the calibration which minimizes the effect of systematic errors in the relative spectra was therefore adopted.

All known absolute measurements of the flux density of Cass A were compiled and after correcting for an assumed secular decrease of 1 per cent per year in the flux density, these results were used to determine an absolute spectrum of Cass A. This list of absolute calibrations is somewhat less extensive than that compiled by others. This is due to the greater restrictions put on the definition of "absolute calibration". Only those measurements were used which involved an experimental determination of the antenna collecting area or where the area could be accurately calculated, and where a careful measurement was made of the receiver sensitivity.

As can be seen from Figure 1a, the points are consistent with the assumption that the spectrum of Cass A is closely approximated by a power law with a spectral index of -0.77 as determined by a least-squares fit of all the observations above 30 Mc. It is evident that below about 30 Mc the observed spectral law changes and the flux density remains approximately constant between 12.5 and 30 Mc. This low frequency cutoff is in all probability due to absorption in ionized hydrogen located in the path of propagation.

The spectrum of Cass A was then used to obtain <u>preliminary</u> calibrations at each frequency where intensity

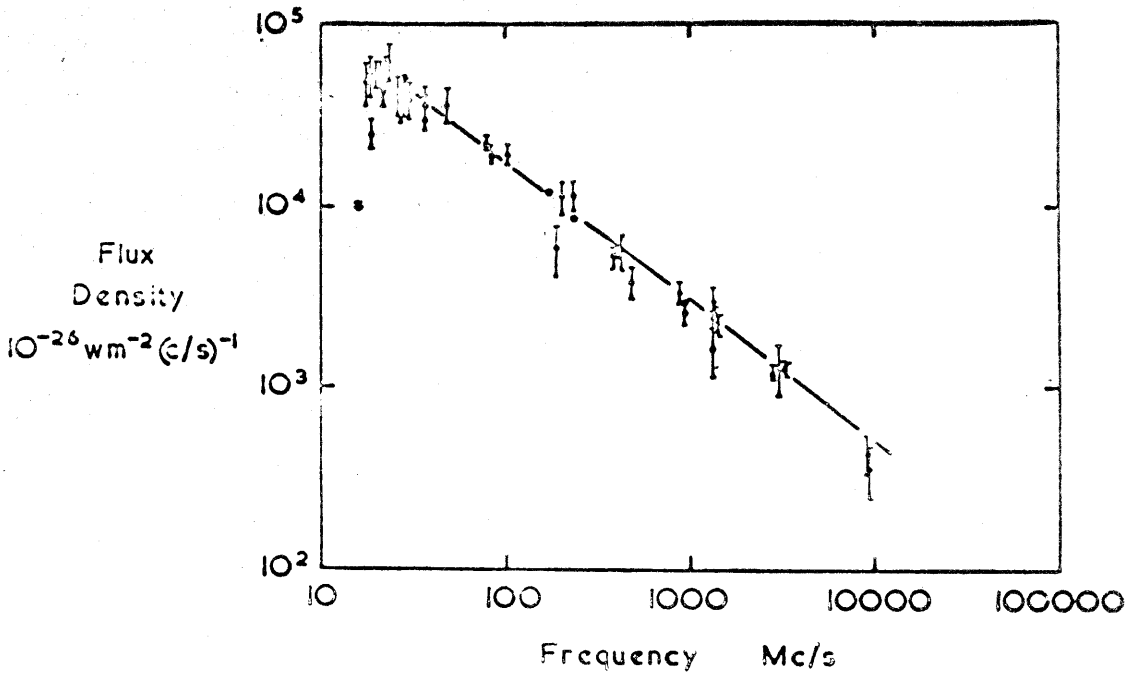

Figure 1a Spectrum of Cass A based on absolute measurements of flux density.

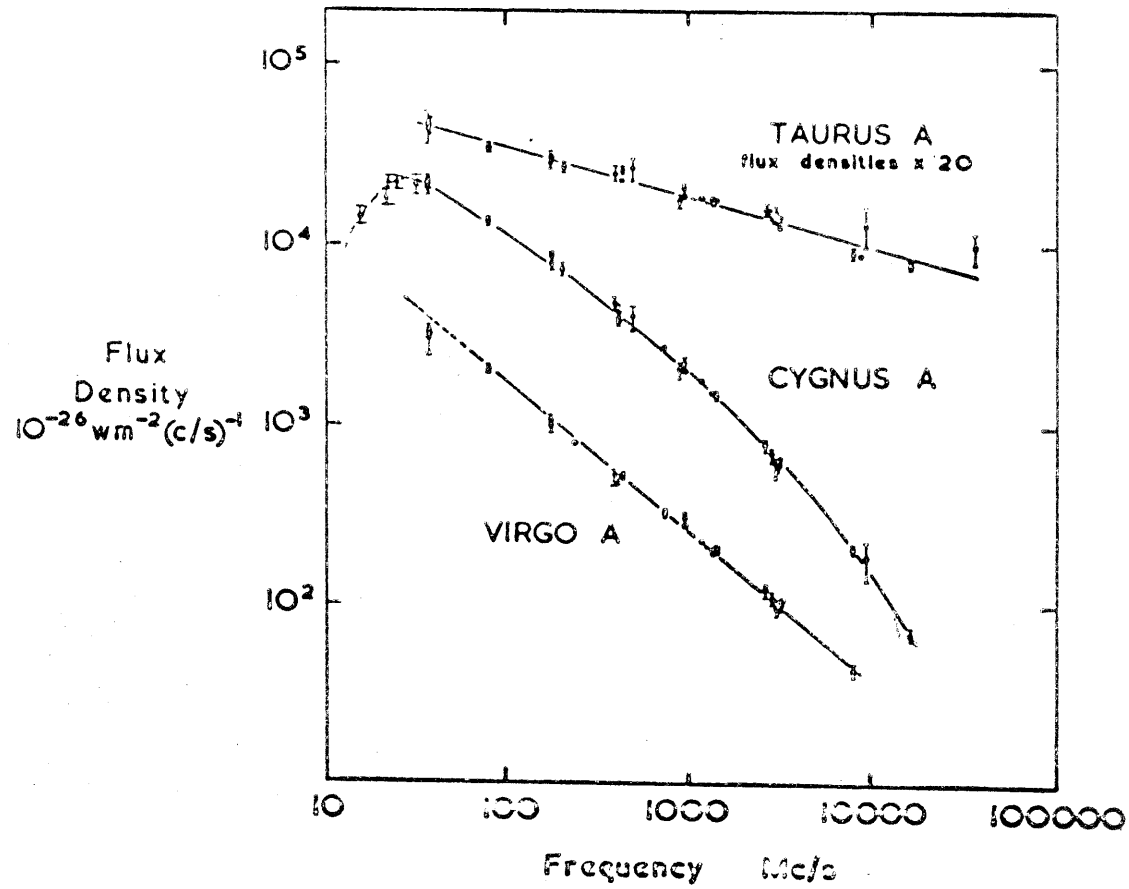

Figure 1b Spectrum of Taurus A, Cygnus A, and Virgo A based on relative measurements of flux density.

ratios to Cass A existed. These were used to determine the spectra of the other three strong sources, Cygnus A, Taurus A, and Virgo A, shown in Figure 1b. These four sources were then established as primary standards for the calibration of the flux density scale at each frequency and the flux of a number of moderately strong sources was then determined at those frequencies where intensity ratios to the primary calibrators were available. These sources are sufficiently intense for the effects of noise fluctuations to be negligible but not so intense as to introduce uncertainties due to non-linearities in the receiver (about 1 per cent of the strength of Cass A). Their angular size was small enough that they were not resolved with the interferometer.

Five such sources whose spectra showed no significant deviations from a power law between 38 Mc and 1420 Mc were then selected as secondary calibrators. The best fitting power law spectrum was then calculated for these sources and this was used to obtain the final calibrations at frequencies between 38 Mc and 1420 Mc.

At 3200 Mc (or 2840 Mc) the observed flux densities showed a fairly large dispersion about the extrapolation of the low frequency spectrum. Since even for the moderately strong sources, the uncertainties due to noise fluctuations are no longer negligible at this frequency, and as there is no a priori reason to assume that the spectral index of the calibration sources remains constant out to centimeter wave-

lengths, the flux density scale at 3200 Mc was determined directly from the observed ratios to Cass A and Taurus A. Since at this frequency the antenna temperature from Cass A is small compared to the system noise temperature, the effects of the receiver non-linearity discussed above are not important.

The calibration of the interferometer measurements at 2840 Mc was obtained by interpolating the spectra of a number of moderately strong sources between 1420 Mc and 3200 Mc. Due to the small frequency difference between the interferometer and pencil beam measurements at 3200 Mc, uncertainties in the spectra of these sources did not significantly affect the calibration at 2840 Mc.

Considering the different calibration technique employed at these frequencies and in view of the uncertainties due to low signal to noise ratio, antenna pointing errors, and the effects of linear polarization which all become important at these frequencies, the quoted results at 10 centimeters must be treated with some caution.

All of the observed flux densities have been corrected for the effects of atmospheric extinction using the expression

$$S(z) = S_o p^{f(z)} \qquad (3.1)$$

where $S(z)$ is the observed value at a zenith angle z, S_o is the true value above the earth's atmosphere, and $f(z)$ is a tabulated function proportional to the number of atoms

of atmosphere in the line of sight. For small values of z, $f(z) \approx \sec z$.

Values of log P estimated from the graphs of Hogg (29)(Table 2) were corrected for the elevation of the observatory and were used to determine the extinction corrections. Graphs of equation 3.1 prepared by A. T. Moffet for 960 Mc and 1420 Mc were used at these frequencies.

Except near the southern horizon, the correction in the relative flux density is less than 0.5 per cent and the uncertainty in this correction is felt to be negligible.

Table 2

Frequency	log P*
475	-.0018
710	-.0024
958	-.0029
1420	-.0032
2840	-.0035
3200	-.0035

*Multiply by 1.16 to reduce to sea level.

The flux densities reported here are twice those observed with the electric vector in position angle zero. In the absence of any linear polarization, this is equivalent to the total flux density of the source. However, recent measurements at Caltech (30)(31) and elsewhere (32) indicate

that the radiation received from many sources is several percent linearly polarized at decimeter wavelengths. As relatively few measurements of polarization are yet available, no corrections have been made for this effect in determining the spectra.

The measured flux densities are given in Table III along with the estimated standard errors. These estimates include the uncertainty in the resolution and pointing error corrections, as well as effects of noise and confusion. They do not however, include any uncertainty in the calibration of the flux density scale which is believed to be good to within about 5 per cent at each frequency.

Most of the sources are taken from the 3C survey (17), the revised 3C survey (18), the CTA list (4), or the survey of Mills, Slee, and Hill (20)(21). The original designations of the sources have been used except in cases where the source is known by a more common name.

As a check on these results, the data at 710 Mc, 1420 Mc, and 3200 Mc have been compared with recent observations of a limited number of sources by Heeschen at 750 Mc and 3000 Mc (26), and by Goldstein at 1423 Mc (33).

Comparison of the relative intensities obtained by different observers at nearby frequencies showed that in general, the agreement was not as good as would be expected from the individual uncertainties assigned to the measurements. This has also been noticed by Heeschen (25). Until the cause of these systematic errors is better understood,

Table III

Source	475 Mc	710 Mc	958 Mc	1421 Mc	2841 Mc	3200 Mc	Notes
3C 2			4.8 ± 0.3	3.4 ± 0.2			
3C 5			2.3 0.4	1.8 0.3			a
MOO-2 9			3.6 0.3	3.1 0.2			
3C 10	84.4 ± 8.4	67.9 ± 1.8	55.1 0.9	43.4 1.3		29.0 ± 3.0	b
MOO-2 10	17.2 1.7	14.0 0.5	10.0 0.4	8.1 0.4	2.9 ± 0.4		c
3C 15			5.7 0.3				d
3C 17	13.2 1.6	10.7 0.5	7.8 0.4	5.0 0.3			d
3C 18			6.0 0.5	3.7 0.6			
3C 19		5.6 0.5	4.4 0.4	3.2 0.3			
MOO-4 10			5.0 0.4	4.3 0.9			
3C 20	22.9 2.5	19.0 0.6	14.7 0.4	10.9 0.3	6.6 0.5	4.7 0.5	
MOO-4 11			10.8 0.4	8.0 0.7			e
NGC 253	16.6 3.3	8.4 1.8	7.2 0.9	5.6 1.3	2.9 0.5		f
3C 23			2.7 0.7				g
CTA 6		19.9 3.0	17.2 1.8	17.3 6.0			h
3C 26			3.1 0.6	2.2 0.4			g
3C 27	16.1 1.8	13.6 0.5	9.9 0.4	7.2 0.2	3.3 1.0		
3C 28			2.6 0.3	1.7 0.2			
3C 29			8.9 0.9				j
3C 32		7.1 0.5	5.6 0.3	3.6 0.3			
3C 33	29.0 1.9	22.9 0.6	18.0 0.5	12.2 0.3	6.8 0.4	6.1 0.7	
3C 38		7.7 0.5	5.9 0.3	3.3 0.4			
3C 40	14.8 1.7	11.5 0.5	9.1 0.4	6.3 0.3			
3C 41		6.4 1.4	4.0 0.4	3.4 0.3			k
3C 43			3.7 0.3	3.0 0.3			
3C 46			3.5 0.8	2.5 0.5			
3C 47		8.6 0.5	5.8 0.3	4.0 0.2			

Table III (continued)

Source	475 Mc	710 Mc	958 Mc	1421 Mc	2841 Mc	3200 Mc	Notes
3C 48	34.0 ± 1.5	26.3 ± 0.6	21.0 ± 0.4	15.6 ± 0.3	8.2 ± 0.4	8.4 ± 0.9	
3C 55			4.2 0.3	2.7 0.2			
MO1-3 15			5.2 0.3	3.8 0.3			
3C 58	36.7 2.8	36.7 3.6	32.5 1.6	34.2 3.9		33.5 4.0	
3C 62			8.1 1.0	6.2 0.8			g
3C 63			5.1 0.3	3.3 0.2			
3C 65			4.8 1.0	3.7 0.8			g
3C 66	21.8 1.6	15.2 0.5	12.6 0.5	9.4 0.4		6.3 1.0	
3C 69		6.5 0.5	5.1 0.4	3.5 0.3			
MO2-1 10			6.2 0.3	4.7 0.2			
3C 71	9.6 1.0	7.5 0.4	6.3 0.5	4.9 0.2	3.7 0.5		g
3C 75	14.3 1.6	9.6 0.5	8.2 0.3	5.9 0.3			
3C 78		11.4 1.6	9.8 1.0	6.9 0.4	5.2 0.5		
3C 79		9.2 0.5	6.5 0.3	4.6 0.2			
CTA 21	10.3 1.4	9.2 0.5	9.2 0.3	7.8 0.3	4.2 0.3		
3C 84	25.8 1.6	20.4 0.8	18.0 0.6	13.0 0.4	7.4 0.5	8.9 0.6	
Fornax A			145. 11.6				1
3C 86		13.3 1.3	11. 0.8	8.9 1.0			
3C 88			7.0 0.5	6.0 0.4			
3C 89			6.2 0.7	4.9 0.7			
CTA 26			2.1 0.3	1.9 0.2	2.8 0.4		g
MO3-1 9			4.8 0.3	3.5 0.5			
MO3-2 12	15.0 1.3	10.3 1.1	7.7 1.1	5.6 0.7			
3C 98	23.1 1.3	17.2 0.6	14.1 0.4	9.8 0.3	6.7 0.5	6.2 0.7	
3C 103		9.5 0.5	7.0 0.3	5.2 0.3			
3C 105			7.5 0.5	5.9 0.7			
MO4-1 2	9.4 1.4	5.2 0.5	3.9 0.3	3.0 0.4			
NPC			4.1 0.3	1.9 0.3			

Table III (continued)

Source	475 Mc	710 Mc	958 Mc	1421 Mc	2841 Mc	3200 Mc	Notes
3C 109		7.2 ± 0.5	6.1 ± 0.3	3.9 ± 0.2			
MO4-2 4			3.8 0.5	2.8 0.4			
3C 111	34.1 ± 2.2	25.5 1.1	20.1 0.6	15.2 0.8	9.8 ± 1.0	8.2 ± 0.5	
3C 119	16.8 1.6	12.4 0.5	9.9 0.5	8.5 0.2	4.7 0.5		n
MO4-1 12			2.8 0.4				
3C 123	110.2 4.8	79.1 1.5	60.5 1.2	46.2 1.0	24.3 1.5	22.3 1.4	
MO4-2 18			10.3 0.5	7.0 0.3			
HB 9			155.2 30.0				l
3C 131			4.0 0.4	2.7 0.3			p
3C 132			4.5 0.4	3.1 0.3			g
3C 133		10.7 2.1	8.1 1.7	6.3 1.4	3.1 0.5		g
3C 134	31.1 2.4	20.3 1.1	14.6 0.8	9.5 0.6	3.9 0.4		
3C 135			4.5 0.5	3.1 0.7			
MO5-4 2			5.9 1.0				
MO5-0 3			5.5 1.4	1.8 0.4			c
3C 138			11.6 0.7	9.7 0.4	6.5 0.6		
Pictor A	140.6 15.4	119.5 13.2	85.8 3.5	68.1 10.5			
MO5-3 6	31.4 1.6	25.5 0.8	20.2 0.6	14.3 1.6	7.7 0.7		
3C 141			3.6 0.6				
3C 142.1			4.3 0.9				
3C 144						710. 40.	
3C 145			350. 10.			340. 20.	
3C 147	43.5 2.5	34.7 1.6	28.7 0.6	21.4 0.5	11.6 0.8	11.4 0.8	
3C 153	10.2 1.6	7.1 0.5	5.1 0.4	4.1 0.3			r
3C 154	12.1 1.1	8.4 0.5	7.0 0.5	4.9 0.2			
3C 157			190. 25.				l
3C 158			3.2 0.3	2.3 0.3			

Table III (continued)

Source	475 Mc	710 Mc	958 Mc	1421 Mc	2841 Mc	3200 Mc	Notes
3C 159			4.1 ± 0.5	2.6 ± 0.4			
3C 161	40.0 ± 1.4	30.0 ± 0.6	24.7 0.5	18.7 0.4	10.4 ± 0.5	9.3 ± 0.6	
3C 163			330. 36.				l
MO6-2 10	18.5 1.4	9.8 0.5	10.2 0.4	6.7 0.3			j
3C 166			3.3 0.3	2.7 0.2			s
3C 171		6.5 0.4	5.3 0.3	3.6 0.3	2.4 0.4		
MO6-2 16		6.6 0.5	4.8 0.3	3.2 0.2			
3C 172			4.2 0.4	2.9 0.3			
3C 175			4.0 0.3	2.5 0.2			
3C 178			2.0 0.3	1.4 0.2			
3C 180			3.8 0.3	2.7 0.2			
3C 184			2.1 0.3	1.1 0.4			
3C 187			2.5 0.3	1.6 0.2			
MO7-1 17		7.3 0.6	5.4 0.6	3.3 0.6			
3C 191			2.8 0.3	1.6 0.2			
3C 192	11.1 1.4	7.8 0.5	6.5 0.3	4.8 0.2			
3C 195		6.3 0.5	5.8 0.4	3.9 0.3			
3C 196	36.0 1.2	25.5 0.6	20.0 0.4	14.4 0.4	7.4 0.7	7.3 1.5	
3C 198			3.2 0.3	2.2 0.3			
Puppis A			128. 12.				l
3C 202		3.4 0.8	3.0 0.7	1.8 0.5			t
3C 208			4.7 1.0	3.6 0.8			g
3C 212		4.5 0.5	3.3 0.4	2.6 0.3			u
CTB 31			242. 50.				c
MO8-2 19		10.5 0.5	7.9 0.4	5.8 0.6	2.7 0.4		
3C 216	10.2 1.1	6.6 0.5	5.4 0.3	4.0 0.2			
3C 218	118.0 5.1	82.8 3.2	62.0 2.8	42.6 2.2	18.9 1.1	16.8 1.5	
3C 219	23.8 1.4	15.4 0.4	11.8 0.3	8.2 0.6	4.5 0.4	3.6 0.5	

Table III (continued)

Source	475 Mc	710 Mc	958 Mc	1421 Mc	2841 Mc	3200 Mc	Notes
3C 225		8.3 ± 0.8	6.5 ± 0.7	4.3 ± 0.6			
3C 227	18.0 ± 2.1	12.8 0.5	9.8 0.5	7.3 0.3	4.1 ± 0.4		
3C 228		8.0 0.6	5.2 0.3	3.3 0.2			
3C 230			5.7 0.4				
3C 231	13.1 1.3	10.8 0.6	9.5 0.4	8.6 0.4	6.2 0.6	6.5 ± 2.0	
3C 234		11.5 1.0	7.9 0.3	5.6 0.3	6.2 0.8		
M10-2 1	6.2 1.2	4.9 0.4	3.1 0.3	2.2 0.2			
3C 237	13.9 1.1	10.7 0.5	9.3 0.3	6.2 0.2	3.7 0.4		
3C 238			5.3 0.6	3.0 0.5			g
M10-4 4		8.7 0.5	7.7 0.9	4.3 0.6			
3C 243		4.6 0.9	2.1 0.5	1.4 0.4			g
3C 245			4.3 0.3	3.3 0.2			
3C 249			4.3 0.3	2.9 0.3			
3C 254		5.5 0.7	4.3 0.5	3.0 0.3			g
3C 261			1.7 0.3	1.1 0.2			
M11-1 8		8.4 0.5	6.6 0.4	5.3 0.4			
3C 264		10.5 0.4	7.9 0.3	6.0 0.3	4.2 0.4		
3C 265			4.6 0.3	2.8 0.2			
3C 267			3.2 0.3	1.9 0.2			
3C 270	37.3 3.1	31.4 4.6	27.5 1.3	20.7 3.1		9.1 0.5	h
M 84	14.7 5.1	9.9 1.0	7.9 0.3	5.9 0.2	4.4 0.4	4.3 0.6	v
3C 273	52.3 1.8	48.6 1.3	43.1 1.2	38.6 0.8	33.5 2.1	31.2 2.5	
M 87			290. 15.			107. 10.	l
3C 275			4.1 0.3	1.8 0.2			
Coma A		3.9 0.5	3.2 0.4	3.2 0.3			w
3C 278	13.0 1.9	12.1 0.5	9.8 0.4	7.5 0.3	4.4 0.4		
3C 279	11.5 1.2	8.5 0.8	8.4 0.5	6.2 0.4	4.6 0.4		g
3C 280	11.8 1.5	10.0 0.8	6.9 0.3	5.2 0.2			

Table III (continued)

Source	475 Mc	710 Mc	958 Mc	1421 Mc	2841 Mc	3200 Mc	Notes
3C 283	17.2 ± 1.1	10.6 ± 0.5	7.8 ± 0.3	4.8 ± 0.2	2.5 ± 0.3		
NGC 5128C			428. 75.				l
3C 286	23.8 1.4	20.7 1.1	18.6 0.4	15.5 0.3	10.8 0.4	9.5 ± 1.5	
3C 287	12.4 1.3	8.8 0.6	8.1 0.5	6.8 0.3	4.4 0.4		x
M13-0 11			4.0 0.8	2.2 0.4			
3C 295	52.3 4.9	36.2 0.9	31.0 0.8	22.4 0.5	11.0 0.8	10.7 0.8	
3C 298	22.8 1.0	13.2 0.5	9.4 0.3	5.6 0.2	2.4 0.4		
3C 299		4.9 0.6	4.2 0.3	2.9 0.2	1.6 0.4		
3C 300.1			3.1 0.4	2.3 0.4			
M14+0 10			3.5 0.5	2.3 0.4			y
M14-1 21		6.4 0.5	5.5 0.3	3.4 0.2			
3C 309.1		12.1 0.6	10.2 0.4	8.0 0.3	5.2 0.5		
M14-4 15		4.2 1.0	3.2 0.8	1.9 0.4			
3C 310	25.1 1.4	15.6 0.6	11.8 0.4	7.3 0.3	3.5 0.4		
3C 313			5.5 0.3	3.5 0.2			c
3C 315		6.9 0.6	5.8 0.4	4.1 0.3			
3C 317		13.5 0.6	9.6 0.4	5.6 0.3	2.5 0.4		
M15-0 5			4.1 0.5		2.3 0.4		
3C 318			3.7 0.3	2.6 0.2			
3C 318.1			2.8 0.8				
3C 319			3.5 0.4	2.5 0.3			
M15-4 3	12.8 1.4	9.1 0.5	6.7 0.4	3.7 0.4			
3C 324			3.9 0.3	2.5 0.2			
3C 327	24.6 1.6	13.4 0.6	11.5 0.5	8.0 0.4			z
3C 327.1	15.1 1.3	7.4 0.5	5.9 0.5	3.6 0.3			z
M16+0 3			2.9 0.3	2.4 0.3			z
NPC				4.9 0.5	2.2 0.2		

Table III (continued)

Source	475 Mc		710 Mc		958 Mc		1421 Mc		2841 Mc		3200 Mc		Notes
3C 330			12.4	± 1.1	9.3	± 0.6	6.6	± 0.3					
3C 332					3.7	0.7	2.4	0.4					
3C 334					3.2	0.4	2.4	0.3					
M16-1 8					2.6	0.3	2.3	0.3					
3C 338	16.7	± 1.6	9.5	0.5	6.3	0.3	3.6	0.2	1.6	± 0.4			
M16-4 7					329.8	70.0							
3C 345	9.6	1.0	8.5	0.5	7.8	0.3	6.6	0.3	5.7	0.8	4.5	± 0.5	
3C 347					2.4	0.6							g
Her A	130.3	3.1	88.5	2.2	68.0	2.9	46.4	1.8	22.8	1.9	19.3	1.0	
3C 353	118.0	4.1	88.9	1.4	74.7	1.8	56.7	1.3	28.7	3.0	26.1	1.4	
3C 358	30.9	2.1			18.9	0.4	15.2	0.5			9.5	1.2	
M17-3 9	51.9	2.1	34.2	1.5	26.7	0.6	21.7	0.5					
3C 365					3.3	0.7	1.5	0.4					g
M17-2 16					291.	60.							l
M17-2 17					6.2	1.2	5.2	1.1					
M18-2 1					203.	40.							u
M 17					485.	75.							u
M18-1 8					203.	40.							u
3C 380	30.3	2.5	23.6	0.6	18.2	0.5	14.2	0.8	8.5	0.4	8.9	0.5	
M18-0 8					77.	15.							
CTA 80			8.2	0.5	7.5	0.4	6.0	0.3					
3C 386	15.0	2.9	10.8	0.5	9.0	0.4	7.3	0.3	4.0	0.4			
3C 387					10.0	0.4							
M18-4 3					4.1	0.4	2.6	0.3					
3C 388	14.9	2.9	10.5	0.5	7.8	0.4	5.8	0.2	3.6	0.4			
3C 389					6.7	0.6	5.6	0.6					
3C 390			8.3	0.6	6.7	0.5	4.6	0.4					
3C 390.3	24.9	6.7	17.7	0.7	13.1	0.5	10.0	0.5	6.1	0.7			

Table III (continued)

Source	475 Mc		710 Mc		958 Mc		1421 Mc		2841 Mc		3200 Mc		Notes
3C 391	38.6	± 8.2	22.9	± 3.0	19.9	± 2.0	9.7	± 1.1					
3C 392					204.7	9.0							1
3C 394					4.4	0.6							
3C 396			18.4	0.7	15.7	0.9	11.6	1.5					
3C 398					89.2	14.0							
3C 400					436.	90.							
M19-4 6	34.5	5.1	22.8	0.8	15.9	0.6	11.9	0.5					
M19-1 11					7.1	0.4	5.3	0.4					
3C 401	12.2	3.7	8.0	0.5	6.7	0.5	5.2	0.4					
3C 402					4.8	1.0	3.7	0.5					g
3C 403			9.9	0.5	7.8	0.4	5.9	0.3	3.7	± 0.4			g
3C 405											630.	±30.	
3C 409	37.4	7.4	26.2	0.9	19.0	0.5	13.2	0.3	5.1	0.4	4.4	0.3	
CTB 87			18.4	0.9	8.7	0.5	8.8	0.9					
3C 410	22.9	5.1	16.3	0.5	13.1	0.5	10.7	0.2	6.0	1.6	5.4	0.4	
3C 411					4.6	0.3	2.8	0.2					
M20-3 7	13.4	4.1	9.7	0.5	7.3	0.4	5.2	0.3					
3C 418			6.6	0.5	5.7	0.3	5.1	0.2	3.9	0.7			
HB 21					155.	30.							1
3C 424			4.7	0.5	3.4	0.3	2.5	0.2					
M20-2 14					3.4	0.3	2.5	0.2					
M21-2 1	26.6	5.5	17.9	0.6	15.1	0.4	10.7	0.3	4.4	0.6			
M20-2 15			10.1	0.8	6.9	0.5	5.3	0.2					
3C 427.1					5.4	0.8	3.3	0.5					
3C 428					2.8	0.4	2.2	0.4					
3C 430	14.9	4.6	11.9	0.5	9.4	0.4	7.4	0.3	4.4	0.4			
3C 431	11.7	2.6	6.2	0.5	4.5	0.3	2.7	0.2					

Table III (concluded)

Source	475 Mc	710 Mc	958 Mc	1421 Mc	2841 Mc	3200 Mc	Notes
3C 433	32.5 ± 4.1	22.4 ± 0.9	16.1 ± 0.5	11.6 ± 0.5	6.3 ± 0.4	5.6 ± 0.5	
M21-4 7			3.9 0.3	2.7 0.2			
3C 436			4.7 0.5	3.4 0.4			g
3C 437			3.3 0.3	2.6 0.2			
CTA 97			4.4 0.6	5.1 2.5			
3C 438	19.9 3.6	14.4 0.5	9.9 0.5	6.7 0.2	3.4 0.4		
3C 441			4.0 0.3	2.5 0.2			
3C 444	22.6 5.3	18.1 0.6	12.5 0.4	7.7 0.3	3.7 0.4		
3C 442			4.9 0.4	3.0 0.3			g
3C 445	11.8 2.6	10.8 0.5	7.2 0.3	6.8 0.4			g
3C 446			7.9 0.4	5.8 0.4			
CTA 102		7.3 0.5	7.2 0.3	6.4 0.3	4.7 0.4		
3C 452	29.3 6.3	20.3 0.5	14.8 0.4	10.7 0.3	6.2 0.4	6.6 0.4	
3C 454.1		12.7 0.7	12.8 0.6	11.3 0.5	9.3 0.4		bb
M22-4 6		9.0 0.5	5.8 0.4	3.9 0.2			
3C 456			3.3 0.9				j
3C 458			3.3 0.3	1.9 0.3			
3C 459		8.5 0.5	6.2 0.3	4.4 0.2			
M23-1 12		4.3 0.6	2.7 0.5	1.7 0.4			
Cass A						1330. 70.	
M23-4 3			3.4 0.5	2.7 0.5			
M23-4 4		10.2 0.5	6.7 0.4	5.0 0.2			
3C 465	20.2 4.6	15.2 0.6	10.7 0.5	7.9 0.4	3.3 0.4		

Notes to Table III

3C - Third Cambridge Catalogue (17) or Revised 3C Catalogue (18).
M - Sydney Catalogue (20),(21).
CTA - Harris and Roberts (4).
CTB - Wilson and Bolton (91).
NPC - Not Previously Catalogued.

a) Confused with 3C 4 and 3C 6.
b) Possibly part of an extended source.
c) Listed by MSH (20),(21) as possibly extended.
d) Several sources in this region including MSH 00-0 9
e) Size uncertain - could be resolved.
f) Unusually large disagreement among various observers.
g) Interferometer measurements indicate some large scale structure.
h) Heavily resolved - large correction necessary.
j) Listed by MSH (20),(21) as extended - interferometer measurements indicate some large scale structure.
k) Confused with source at $\alpha(1950)=01^h25^m12^s.1$, $\delta(1950)=+36^o26'.6$.
l) 958 Mc flux density from Harris and Roberts (4).
m) $\alpha(1950)=04^h07^m02^s$, $\delta(1950)=+74^o43'$.
n) Confused with source at $\alpha(1950)=04^h25^m47^s.8$, $\delta(1950)=+42^o26'.9$.
p) Confused with source at $\alpha(1950)=04^h29^m18^s.2$, $\delta(1950)=+31^o53'.9$.
q) Confused with source at $\alpha(1950)=04^h52^m26^s.3$, $\delta(1950)=+23^o06'.2$.
r) Confused with source at $\alpha(1950)=06^h08^m16^s.9$, $\delta(1950)=+47^o58'.4$.
s) Listed by MSH as extended.
t) Confused with 3C 201.
u) 958 Mc flux density from Wilson and Bolton (91).
v) 475 Mc observations confused by M 87.
w) Confused with source at $\alpha(1950)=12^h51^m42^s.9$, $\delta(1950)=+26^o43'.3$.
x) Confused with source at $\alpha(1950)=13^h28^m58^s.4$, $\alpha(1950)=+25^o.04'.8$.
y) Two sources at $\alpha(1950)=14^h34^m26^s.4$, $\delta(1950)=03^o43'.3$; $\alpha(1950)=14^h35^m50^s.8$, $\delta(1950)=03^o58'.1$.
z) 3C 327 (MSH 16+0 1), 3C 327.1 (MSH 16+0 2), MSH 16+0 3, and a source at $\alpha(1950)=16^h02^m33^s$, $\delta(1950)=+00^o42'$.
aa) $\alpha(1950)=16^h07^m20^s$, $\delta(1950)=26^o51'$.

All flux densities are in units of 10^{-26} W/m^2/cps.

it seems unrealistic to assign uncertainties of less than 5 per cent when comparing results of different observers using different techniques.

One obvious possible cause of such discrepancies is the presence of a small amount of linear polarization. Thus the measured flux density would depend on the angle of the plane of polarization with respect to the polarization of the antenna. This problem could be avoided by properly combining the results obtained in two orthogonal planes of polarization or by using circular polarized feeds. Such an arrangement would then give a result proportional to the total intensity of the source and independent of the degree or direction of any linear polarization.

In order to extend the frequency range beyond that available to the Caltech instrument, data from other studies of the intensity of radio sources were included in the determination of the spectra. The references to these observations are given in Table IV.

In each case the flux density scale has been multiplied by some constant factor in order to make the calibration consistent with that used for the Caltech observations. Where the individual observers do not give any estimate of the uncertainty in their results, or where they only give the internal error, this was estimated by the present author using a similar procedure as used for the Caltech measurements.

Table IV

Frequency Mc	Normalization Factor	Reference
38	1.08	34
85.5	.82	20,21
178	1.08	34
240	1.09	34
408	1.07	34
408	1.14	35
412	.97	34
440	5,810*	25
750	3,820*	26
1200	2,650*	25
1390	.78	36
1400	2,400	25
1423	.93	33
3000	1,370*	26
3000	600	25

*Author gives ratio to Cass A.

IV. THE SPECTRA

4.1 Classification

The available data were first inspected in the form of graphical plots of flux density vs. frequency for each source and compared with a power law spectrum of the form

$$(\text{flux density}) \propto (\text{frequency})^{\alpha} \qquad (4.1)$$

where α is termed the spectral index.*

On the basis of these plots, the spectra have been classed in the following categories;

Class S (157 sources) The spectral index is constant within the experimental errors.

Class C (23 sources) The index is a function of frequency over the observed frequency range.

Class T (9 sources) The source has a spectrum that is characteristic of thermal radiation from free-free transitions in an ionized hydrogen region that is optically thin at high frequencies.

---

*There has been a considerable lack of uniformity in the literature in the definition of the sign of the spectral index α. We have chosen to define the spectral index so that it is the slope of the curve in a logarithmic plot of flux density vs. frequency. Thus, the spectral index for most non-thermal sources is negative. In the rest of this work, a comparison of two spectral indices refers to their relative absolute values. That is, an index of -0.7 is said to be larger than an index of 0.0.

Table V

No.	Source	Class	Flux Density* (400 Mc)		Spectral Index		Flux +
1	3C 2	S	9.1	± 0.3	-0.75	± .03	2.5
2	3C 5	S	4.2	0.5	-0.71	.11	1.2
3	M00-2 9	S	7.8	0.8	-0.77	.09	2.1
4	3C 10	S	99.9	2.6	-0.67	.03	29.
5	M00-2 10	C_L	20.	3.			5.5
6	3C 15	--	10.0	0.6	-0.64	.05	3.0
7	3C 17	S (C)	14.7	0.9	-0.70	.07	4.2
8	3C 18	C (S)	11.7	1.0	-0.75	.08	3.2
9	3C 19	S	7.6	0.4	-0.66	.07	2.2
10	M00-4 10	S	9.5	0.5	-0.71	.04	2.7
11	3C 20	S	25.6	1.2	-0.64	.06	7.6
12	M00-4 11	S	17.6	0.7	-0.58	.04	5.5
13	M00-2 22	--	10.9	1.1	-0.63	.09	3.3
14	3C 23	S	4.7	0.6	-0.76	.13	1.3
15	CTA 6	T	15.	3.			
16	3C 26	S	5.6	0.5	-0.66	.09	1.6
17	3C 27	S	18.6	1.0	-0.71	.06	5.2
18	3C 28	S	6.7	0.3	-1.13	.03	1.8
19	3C 29	S	15.6	2.1	-0.60	.17	4.8
20	3C 32	S	11.3	0.4	-0.84	.04	3.0
21	3C 33	C (S)	32.1	0.7	-0.71	.03	9.0
22	3C 38	S	11.3	0.7	-0.79	.07	3.0
23	3C 40	S	18.1	0.6	-0.82	.03	4.8
24	3C 41	S	7.6	0.6	-0.60	.07	2.3
25	3C 43	S	7.4	0.3	-0.71	.05	2.1
26	3C 46	S	6.6	0.3	-0.66	.03	1.9
27	3C 47	S	12.9	0.5	-0.89	.04	3.4
28	3C 48	C_L	38.	3.	-0.52	.06	11.
29	3C 55	S	9.2	0.7	-0.94	.07	2.4
30	M01-3 15	S	8.6	0.5	-0.61	.05	2.6
31	3C 58	S (T)	32.4	1.9	0.06	.07	24.
32	3C 62	--	12.9	1.3	-0.58	.08	4.0
33	3C 63	S	10.9	1.0	-0.91	.08	2.8
34	3C 65	S	12.9	1.0	-1.05	.09	3.4
35	3C 66	S	24.0	1.3	-0.71	.06	3.7
36	3C 69	S	10.9	0.6	-0.86	.06	2.9
37	M02-1 10	S	11.3	0.6	-0.70	.05	3.2
38	3C 71	S	10.4	0.3	-0.59	.03	3.2
39	3C 75	S	15.1	0.3	-0.73	.02	4.2
40	3C 78	S	12.9	0.5	-0.45	.04	4.6
41	3C 79	S (C)	13.3	0.7	-0.80	.05	3.6
42	CTA 21	C_L	10.5	0.6	-0.06	.08	5.5
43	3C 83-1	--	11.3	1.0	- .57	.10	3.3

Table V(continued)

No.	Source	Class	Flux Density* (400 Mc)		Spectral Index		Flux+
44	3C 84H	S	26.3	± 2.1	-1.25	± .10	3.1
	3C 84C	S	29.2	0.8	-0.62	.03	8.8
45	Fornax A	S	279.	10.	-0.73	.04	77.
46	3C 86	C (S)	18.9	1.2	-0.53	.09	6.2
47	3C 88	S	12.1	0.5	-0.58	.04	3.8
48	3C 89	S	12.6	1.0	-0.79	.06	3.4
49	CTA 26	--	2.9	0.2	-0.34	.10	1.2
50	M03-1 9	S	10.0	0.2	-0.83	.03	2.6
51	M03-2 12	S	15.3	0.7	-0.72	.05	4.3
52	3C 98	S	25.7	0.6	-0.74	.03	7.1
53	3C 103	S	15.5	0.5	-0.88	.03	4.0
54	3C 105	S	11.8	0.3	-0.54	.03	3.8
55	M04-1 2	S	8.4	0.5	-0.82	.06	2.2
56	3C 109	S	11.7	0.4	-0.81	.03	3.1
57	M04-2 4	S	7.0	0.2	-0.72	.03	2.0
58	3C 111	S	38.5	1.1	-0.74	.03	11.
59	3C 119	C_L	14.8	1.1	-0.41	.08	5.5
60	M04-1 12	--	6.7	1.0	-1.00	.08	1.7
61	3C 123	S	118.	2.	-0.74	.01	33.
62	M04-2 18	S	19.9	0.9	-0.80	.05	5.3
63	3C 131	S	8.4	0.4	-0.90	.03	2.2
64	3C 132	S	8.2	0.2	-0.74	.03	2.3
65	HB 9	S	140.	10.	0.16	.10	7.1
66	3C 133	S	14.7	0.9	-0.67	.05	4.3
67	3C 134	S	35.2	1.0	-1.00	.03	9.1
68	3C 135	S	8.9	0.5	-0.81	.05	2.4
69	M05-4 2	--	11.1	1.5	-0.72	.10	3.1
70	3C 138	S	15.9	0.3	-0.38	.02	6.1
71	Pictor A	S	161.	5.	-0.69	.03	46.
72	M05-3 6	C_L	32.3	2.0	-0.51	.08	11.
73	3C 141	S	7.6	0.3	-0.87	.02	2.0
74	3C 142.1	--	10.5	1.8	-0.79	.16	2.8
75	3C 144	S	1200.	25.	-0.26	.02	540.
76	3C 145	T	210.	15.			
77	3C 147	C_L	46.3	2.3	-0.56	.06	15.
78	3C 153	S	11.1	0.4	-0.80	.04	3.0
79	3C 154	S	13.1	0.2	-0.76	.02	3.6
80	IC 443	S	251.	8.	-0.30	.04	110.
81	3C 158	S	7.5	0.2	-0.96	.02	1.9
82	3C 159	S	8.3	0.3	-0.87	.04	2.2
83	3C 161	C_H	41.5	1.2	-0.61	.03	13.
84	3C 163	T	290.	20.			
85	M06-2 10	S	18.0	1.5	-0.73	.08	5.0

Table V(continued)

No.	Source	Class	Flux Density* (400 Mc)		Spectral Index		Flux+
86	3C 166	S	7.9 ±	0.5	-0.90 ±	.05	2.1
87	3C 171	S	11.9	0.4	-0.95	.04	3.1
88	M06-2 16	S	11.1	0.2	-0.97	.02	2.9
89	3C 172	S	8.0	0.3	-0.77	.04	2.2
90	3C 175	S	8.8	0.3	-0.97	.03	2.3
91	3C 178	S	5.2	0.4	-1.06	.07	1.4
92	3C 180	S	7.9	0.4	-0.84	.04	2.1
93	3C 184	S	5.5	0.5	-1.10	.11	1.5
94	3C 187	S	5.9	0.1	-1.01	.02	1.5
95	M07-1 17	S	11.5	0.5	-0.87	.04	3.0
96	3C 191	S	6.2	0.4	-0.98	.06	1.6
97	3C 192	S	12.4	0.2	-0.75	.02	3.4
98	3C 195	S	10.4	0.4	-0.73	.03	2.9
99	3C 196	C_H	38.3	0.6	-0.73	.02	11.
100	3C 198	S^H	8.3	0.2	-1.09	.03	2.2
101	Puppis A	--	219.	18.	-0.61	.09	66.
102	3C 202	S	5.2	0.3	-0.73	.05	1.4
103	3C 208	S	9.4	0.1	-0.81	.02	2.5
104	3C 212	--	7.9	0.7	-0.91	.09	2.1
105	CTB 31	T	100.	20.			
106	M08-2 19	S	15.1	0.5	-0.72	.04	4.2
107	3C 216	S	11.6	0.7	-0.83	.06	3.1
108	3C 218	S	137.0	2.1	-0.93	.02	3.5
109	3C 219	C (S)	24.4	0.7	-0.80	.03	6.5
110	3C 225	S	13.4	0.8	-0.83	.06	3.6
111	3C 227	S	20.2	0.6	-0.82	.03	5.4
112	3C 228	S	10.8	0.8	-0.86	.06	2.8
113	3C 231	S	12.0	0.7	-0.29	.06	5.2
114	3C 234	S	16.6	0.4	-0.85	.02	4.4
115	M10-2 1	S	8.1	0.3	-1.03	.04	2.1
116	3C 237	C_L(S)	15.4	0.7	-0.67	.05	4.5
117	3C 238	S	9.5	0.7	-0.69	.07	2.7
118	M10-4 4	S	13.3	0.9	-0.76	.07	3.6
119	3C 243	S	5.1	0.9	-0.91	.17	1.3
120	3C 245	S	7.2	0.2	-0.61	.03	2.2
121	3C 249	--	9.0	0.9	-0.85	.11	2.4
122	3C 254	S	10.6	0.5	-0.93	.04	2.7
123	3C 261	S	3.7	0.1	-0.93	.03	1.0
124	M11-1 8	S	12.4	0.2	-0.69	.02	3.5
125	3C 264	S	15.7	0.8	-0.78	.06	4.2
126	3C 265	S	10.0	0.7	-0.92	.07	2.6
127	3C 267	S	6.9	0.4	-0.94	.06	1.8
128	3C 270	C	38.2	1.0	-0.50	.03	13.

Table V(continued)

No.	Source	Class	Flux Density* (400 Mc)		Spectral Index		Flux +
129	M 84	S	13.0	± 0.8	-0.59	± .06	4.0
130	3C 273 T	C*	61.0	1.7	-0.40	.03	23.
131	3C 273 A	--	42.	4.	-0.76		11.
132	3C 273 B	--	21.	3.	+ .17		12.
133	M 87 T	--	558.	6.	-0.82	.01	152.
134	M 87 C	C_L	215.	10.	-0.44	.05	78.
135	M 87 H	S	308.	10.	-1.02	.05	84.
136	3C 275	--	6.8	1.6	-0.77	.26	1.8
137	Coma A	--	7.1	0.7	-0.72	.10	2.0
138	3C 278	S	17.7	1.0	-0.72	.06	4.9
139	3C 279	S	13.0	0.4	-0.54	.04	4.2
140	3C 280	S	13.7	0.5	-0.73	.04	3.8
141	3C 283	C (S)	16.7	1.2	-0.89	.08	
142	NGC 5128 C	C	1100.				240.
	NGC 5128 H	S	2200.	200.	-0.61	.04	620.
143	3C 286	C_L	23.4	0.8	-0.29	.04	10.
144	3C 287	S	12.4	0.5	-0.48	.05	4.3
145	M13-0 11	--	7.5	0.7	-0.88	.08	2.0
146	3C 295	C_L	50.3	1.5	-0.58	.03	16.
147	3C 298	C_L	22.9	1.4	-0.98	.07	5.9
148	3C 299	C_L(S)	7.8	0.6	-0.73	.08	2.2
149	3C 300.1	--	6.8	1.0	-0.78	.14	1.8
150	M14+0 10	--	7.0	0.3	-0.84	.03	1.8
151	M14-1 21	S	10.4	1.0	-0.82	.09	2.8
152	3C 309.1	S	14.7	0.7	-0.44	.05	5.2
153	M14-4 15	S	8.0	0.3	-1.12	.03	2.1
154	3C 310	S (C)	26.9	1.0	-1.00	.04	7.0
155	3C 313	S (C)	11.4	1.1	-0.87	.09	3.0
156	3C 315	S	10.2	0.4	-0.70	.04	2.9
157	3C 317	C_H	22.2	1.2	-0.96	.05	5.7
158	M15-0 5	C_L(S)	4.9	0.5	-0.20	.05	2.4
159	3C 318	S (C)	6.8	0.4	-0.71	.06	1.9
160	3C 318.1	S (C)	5.4	1.4	-1.21	.21	1.6
161	3C 319	S	8.2	0.5	-0.93	.08	2.1
162	M15-4 3	S	16.2	0.6	-1.06	.04	4.2
163	3C 324	S	7.0	0.3	-0.75	.04	1.9
164	3C 327	S	25.0	1.4	-0.85	.06	6.6
165	3C 327.1	--	12.8	1.2	-0.88	.10	3.3
166	M16+0 3	--	6.9	0.6	-0.90	.07	1.8
167	3C 330	S	17.0	0.7	-0.71	.04	4.8
168	3C 332	S	6.7	0.2	-0.75	.03	1.8
169	3C 334	S	6.4	.2	-0.78	.02	1.7
170	M16-1 8	--	5.2	0.5	-0.71	.09	1.5

Table V(continued)

No.	Source	Class	Flux Density* (400 Mc)		Spectral Index		Flux +
171	3C 338	C_H(S)	17.9 ±	1.0	-1.17 ±	.06	4.9
172	M16-4 7	T	310.	20.			
173	3C 345	S	9.2	0.5	-0.25	.06	4.2
174	3C 347	--	5.3	0.2	-0.95	.06	1.4
175	3C 348	S	152.	3.	-0.98	.03	39.
176	3C 353	S	135.	2.	-0.70	.01	38.
177	3C 358	S	33.6	1.0	-0.64	.02	10.
178	M17-3 9	S	51.7	2.8	-0.69	.06	15.
179	M17-2 17	--	11.0	0.3	-0.62	.02	5.9
180	3C 365	--	6.7	1.6	-1.00	.22	1.7
181	M17-2 16	--	448.	22.	-0.35	.04	180.
182	M18-2 1	S (T)	203.	5.			130.
183	M 17	T	250.	40.			
184	M18-1 8		127.	30.			
185	3C 380	S	36.7	0.6	-0.77	.02	10.
186	CTA 80	C*	13.1	0.8	-0.69	.06	3.7
187	3C 386	S	16.3	0.5	-0.67	.03	4.7
188	M18-4 3	S	12.2	0.3	-1.23	.03	3.5
189	3C 388	S	14.8	0.4	-0.71	.02	4.2
190	3C 389	S	13.4	0.7	-0.73	.05	3.7
191	3C 390	--	13.0	0.4	-0.79	.04	3.5
192	3C 390.3	S	27.3	0.6	-0.80	.03	7.3
193	3C 391	C_L	31.	5.			9.4
194	3C 392	S	288.	17.	-0.44	.05	100.
195	3C 394	--	8.0	0.8	-0.69	.09	2.3
196	3C 396	S	26.7	2.1	-0.65	.08	7.9
197	3C 398	T	88.0	10.1			
198	3C 400	T?	480.	150.			
199	M19-4 6	S	34.4	1.5	-0.82	.05	9.1
200	M19-1 11	--	12.0	0.4	-0.62	.03	3.6
201	3C 401	S	11.7	0.4	-0.64	.04	3.4
202	3C 402	S	8.7	0.2	-0.68	.02	2.5
203	3C 403	S	15.6	0.6	-0.76	.04	4.3
204	Cygnus A	C_H	4600.	50.	.80	.03	1500.
205	3C 409	S	43.6	0.9	-0.93	.02	11.
206	CTB 87	T?					
207	3C 410	S	22.9	0.6	-0.61	.03	7.0
208	3C 411	C (S)	8.7	0.5	-0.81	.06	2.3
209	M20-3 7	S	13.1	0.7	-0.69	.05	3.7
210	3C 418	S	9.4	0.6	-0.52	.06	3.1
211	3C 424	S	7.0	0.4	-0.80	.05	1.9
212	HB 21	S	200.	15.	-0.34	.09	1.8

Table V (concluded)

No.	Source	Class	Flux Density* (400 Mc)		Spectral Index		Flux+
213	M20-2 14	S	6.5	± 0.2	-0.75	± .03	1.8
214	M21-2 1	S	27.4	0.6	-0.72	.02	7.7
215	M20-2 15	S	14.6	0.7	-0.79	.04	3.9
216	3C 427.1	S	12.4	0.7	-0.99	.06	3.2
217	3C 428	S	8.8	0.5	-1.19	.06	2.4
218	3C 430	S	19.0	1.2	-0.76	.07	5.2
219	3C 431	S	11.1	0.6	-1.06	.06	2.9
220	3C 433	C_H	31.3	1.2	-0.75	.04	8.6
221	M21-4 7	--	8.1	0.2	-0.86	.02	2.1
222	3C 436	S	9.4	0.2	-0.77	.03	2.6
223	3C 437	--	6.6	0.2	-0.75	.03	1.8
224	CTA 97	T	3.2	1.0			
225	3C 438	C_H	22.0	0.8	-0.89	.04	5.7
226	3C 441	S	7.8	0.4	-0.85	.05	2.1
227	3C 444	C_H	27.3	1.3	-0.93	.05	7.1
228	3C 442	S	10.8	0.6	-0.94	.05	2.8
229	3C 445	S	15.7	0.5	0.74	.04	4.3
230	3C 446	S	12.2	0.5	-0.54	.04	4.0
231	CTA 102	C_L	6.8	0.7	0.01	.10	4.6
232	3C 452	S	30.7	0.6	-0.82	.02	8.2
233	3C 454.1	S	14.8	0.2	-0.21	.02	7.2
234	M22-4 6	--	11.9	1.5	-0.80	.12	3.2
235	3C 456	S	8.1	0.9	-0.76	.12	2.2
236	3C 458	--	6.1	0.5	-0.78	.08	1.7
237	3C 459	S	13.1	0.2	-0.84	.02	3.5
238	Cass A	S	6415.	177.	-0.77	.02	1700.
239	M23-1 12	S	6.4	0.5	-0.91	.08	1.7
240	M23-4 3	--	5.4	0.1	-0.54	.01	1.7
241	M23-4 4	--	13.9	1.3	-0.77	.09	3.8
242	3C 465	S	22.7	0.6	-0.81	.04	6.1

≠ Spectrum flattens with increasing frequency.

* 10^{-26} Watts/meter^2/cps.

\+ 10^{-16} Watts/meter^2.

C Core.

H Halo.

In determining this classification, sources were allocated to Class C only if their spectra showed a significant deviation from a straight line. It is clear that this is somewhat biased in that the weaker sources, which in general have larger errors and where the data is not as complete, tend to fall into Class S.

The classification of each source where sufficient data exists is given in column 2 of Table V. In cases where the classification is not certain, an alternate class has been placed in parenthesis. Each spectral class is discussed below in more detail. Examples of sources in each class are shown in Figures 2, 3, 4a and 4b.

Class S

For all Class S sources the best fitting straight line of the form

$$\log S = \alpha \log f + \text{constant} \qquad (4.2)$$

was computed using a least-squares fit to all of the data between 38 and 1420 Mc. In making this fit, each point was weighted in proportion to the inverse square of the per cent error of the flux density. In order to take into consideration the uncertainty in the calibration of the flux density scale at each frequency, as well as possible systematic errors between different observers as discussed above, weights assigned to each datum were determined from

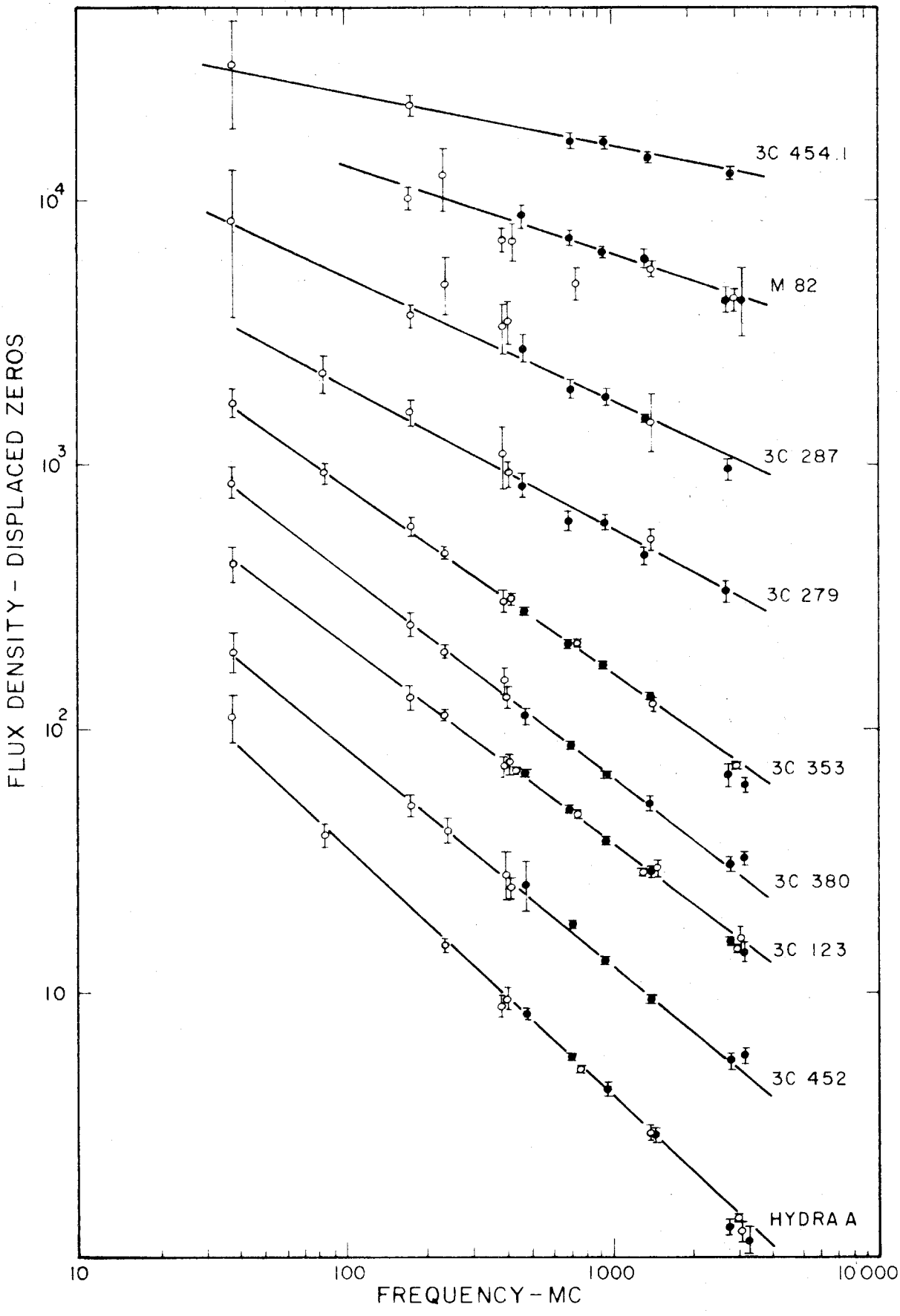

Figure 2 Spectra of some Class S sources.

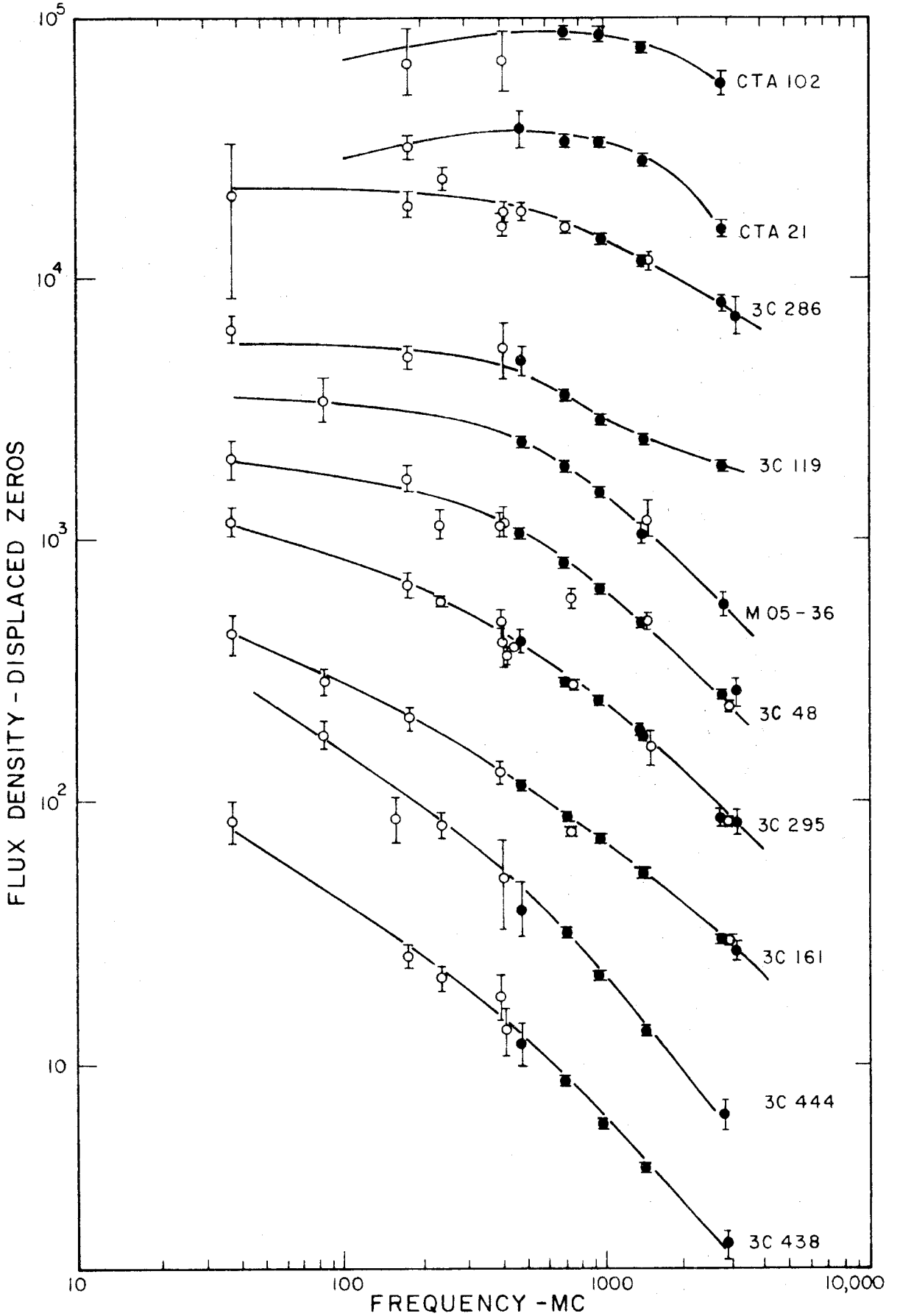

Figure 3 Spectra of some Class C sources.

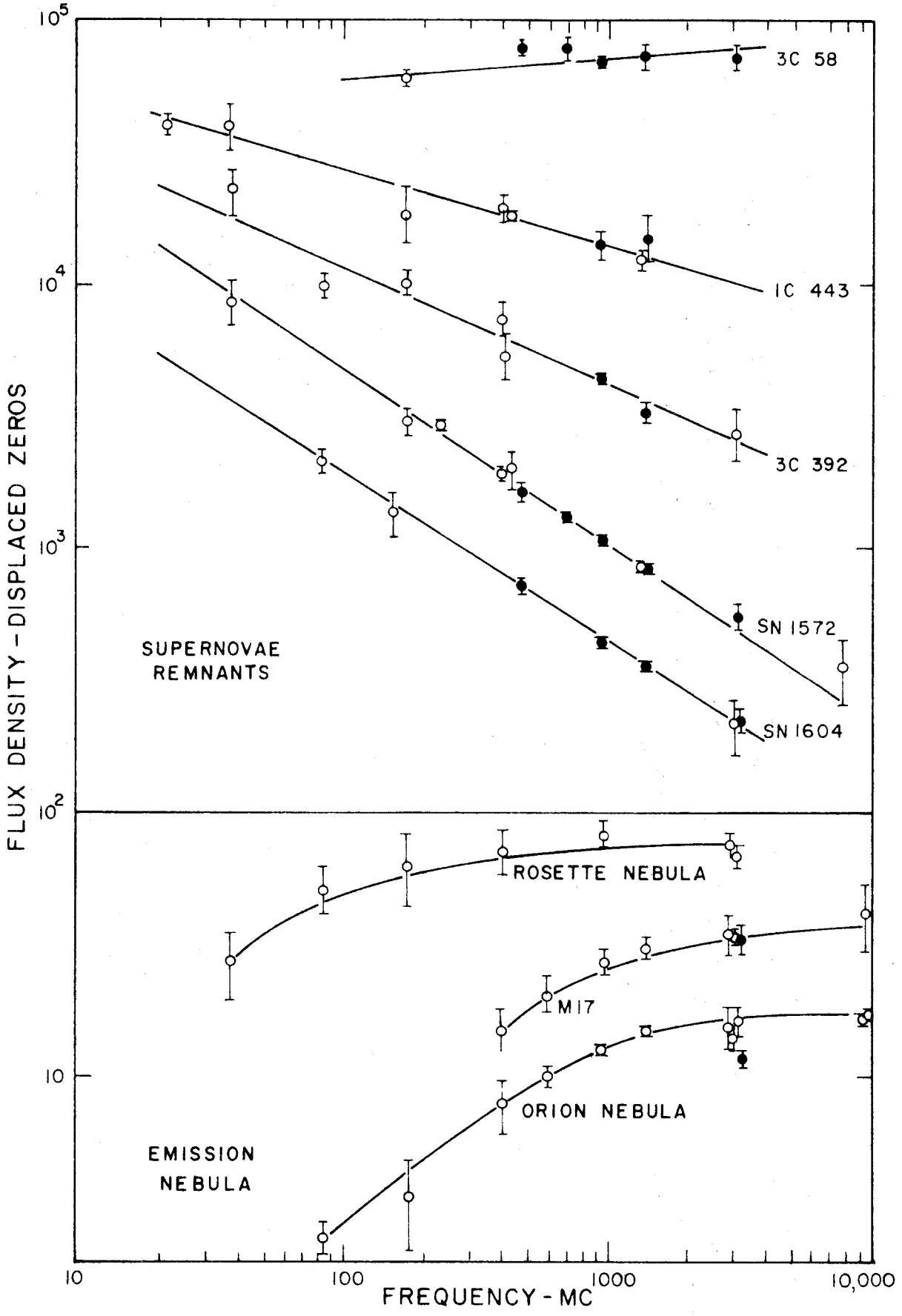

Figure 4 Spectra of some a) supernovae remnants, b) emission nebulae.

the following expression

$$\text{weight} = S^2/(\delta^2 + (.05S)^2) \quad . \qquad (4.3)$$

This allows for an uncertainty of 5 per cent in the intensity scale in addition to the random r.m.s. error, δ in the relative intensities at each frequency.

The values of the spectral index, α, and the flux at 400 Mc computed from the least-squares fit are tabulated in columns 4 and 5 of Table V. The flux density at any other frequency can then be determined from

$$S_f = S_{400}\ (f/_{400})^{\alpha} \qquad (4.4)$$

where f is the frequency in Mc and S_{400} denotes the flux density at 400 Mc.

The distribution of spectral indices for all sources at high galactic latitudes is shown by a histogram in Figure 5a. It is seen to be highly peaked about a median value of -0.76 with a "tail" toward the flat spectra end of the distribution, 50 per cent of the sources having an index between -0.70 and -0.85. As the mean standard deviation in the spectral index for these sources is .05, the observed distribution is only slightly broadened by experimental errors.

The distribution of spectral indices for sources at high galactic latitudes can thus be closely approximated by

$$P(\alpha) = \frac{1}{\sqrt{2\pi}\sigma}\exp -(\alpha - \alpha_o)^2/2\sigma^2 \qquad (4.5)$$

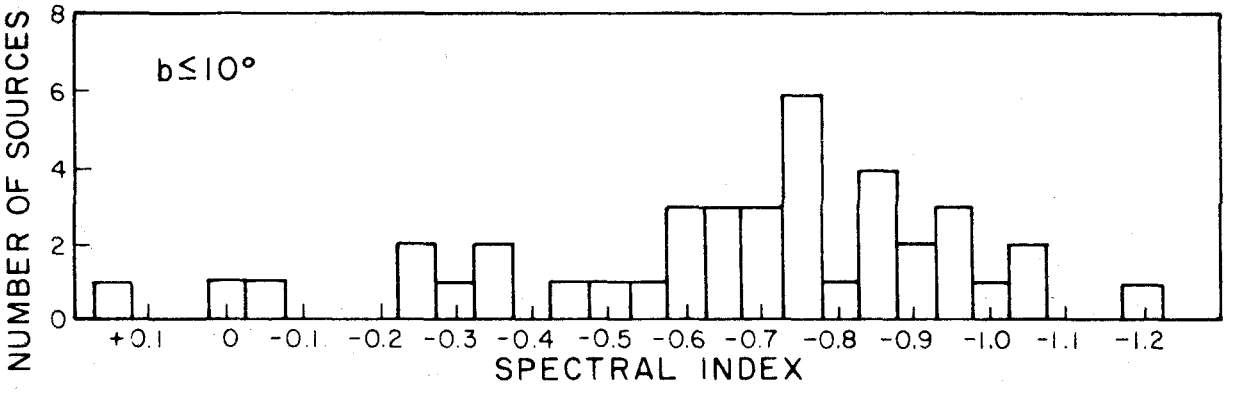

Figure 6 Histogram of spectral indices for "galactic" sources.

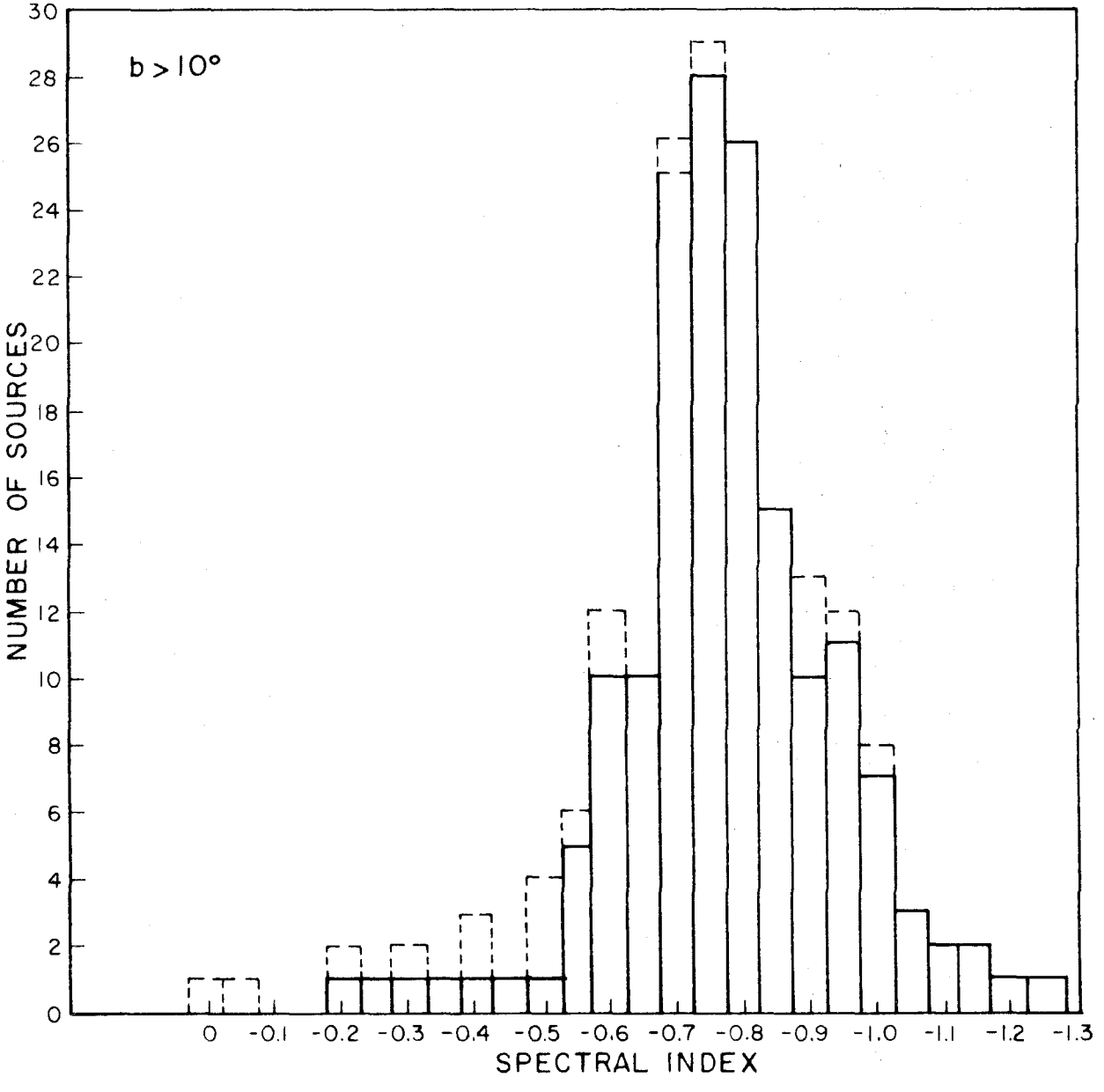

Figure 5 Histogram of spectral indices for "extragalactic" sources. Dotted lines represent curved spectra.

where $P(\alpha)d\alpha$ is the probability of finding a source with a spectral index between α and $\alpha + d\alpha$, $\alpha_o = -0.77$, is the mean spectral index, and $\sigma = .11$, the standard deviation of the dispersion.

This very narrow dispersion is important in that it indicates a similar distribution of electron energies among the sources. In particular we note the complete absence of sources with spectral indices greater than -1.25. Further implications of this result are discussed in Chapter V.

A big step forward in our understanding of the nature of strong radio galaxies would be to find simple relations between their observed physical properties. These could then serve as a basis for the classification of radio sources. It is therefore of interest to compare the spectral characteristics with the results of other studies of radio galaxies.

An obvious beginning is to construct the analogy of a color magnitude diagram relating the spectral index and absolute luminosity. Recently, Heeschen (37) and Pskofsky (38) have suggested such a correlation on the basis of somewhat limited data. As the number of optically identified sources has rapidly increased in the past year, absolute luminosities are now available for some 50 extragalactic sources (See Table VI). In Figure 7 the spectral indices of these sources are compared with their absolute luminosity at 400 Mc. Figure 8 shows a similar comparison with the total radiated power. In both cases we find that a loose

Table VI

Source	Distance Mpc.	P_{400} Watts/cps	Power Watts
3C 15	(250)	7.5×10^{24}	2.3×10^{35}
3C 17	(200)	7.1×10^{25}	2.0×10^{35}
NGC 253	4	2.1×10^{22}	6.3×10^{32}
3C 26	630	2.8×10^{26}	7.7×10^{35}
3C 28	585	2.7×10^{26}	7.3×10^{35}
3C 33	178	1.2×10^{26}	3.4×10^{35}
3C 40	53	6.1×10^{24}	1.6×10^{34}
3C 48	1110	5.1×10^{27}	1.6×10^{37}
3C 63	(650)	5.9×10^{26}	1.5×10^{36}
3C 66	65	1.2×10^{25}	3.4×10^{34}
3C 71	11	1.5×10^{23}	4.6×10^{32}
3C 75	72	9.4×10^{24}	2.6×10^{34}
3C 78	84	1.1×10^{25}	3.9×10^{34}
3C 79	770	9.2×10^{26}	2.6×10^{36}
3C 83.1	54	3.8×10^{24}	1.2×10^{34}
3C 84 C	54	1.0×10^{25}	3.1×10^{34}
H	54	5.9×10^{24}	1.1×10^{34}
3C 88	93	1.2×10^{25}	3.9×10^{34}
NGC 1316	17	9.7×10^{24}	2.7×10^{34}
3C 98	90	2.5×10^{25}	6.9×10^{34}
Pic A	105	2.1×10^{26}	6.1×10^{35}
3C 147	1650	1.5×10^{28}	4.9×10^{37}
3C 171	717	7.3×10^{26}	1.9×10^{36}
3C 198	244	5.8×10^{26}	1.6×10^{35}
Hyd A	159	4.1×10^{26}	1.1×10^{36}
3C 219	522	7.9×10^{26}	2.1×10^{36}
M 82	3.2	1.4×10^{22}	6.2×10^{31}
3C 234	555	6.2×10^{26}	1.6×10^{36}
3C 254	(520)	3.4×10^{26}	8.7×10^{36}
3C 264	63	7.5×10^{24}	2×10^{34}
3C 270	11	5.5×10^{23}	1.9×10^{33}
M 84	11	1.9×10^{23}	5.8×10^{32}
3C 273 A	474	5×10^{26}	3×10^{36}
B	474	1.1×10^{27}	3×10^{36}
M 87 C	11	3.3×10^{24}	1.1×10^{34}
H	11	4.5×10^{24}	1.2×10^{34}
Coma A	258	5.7×10^{25}	1.6×10^{35}
3C 278	43	3.8×10^{24}	1.1×10^{34}
NGC 5128 C	4.7	2.9×10^{24}	6.0×10^{33}
H	4.7	5.8×10^{24}	1.6×10^{34}
3C 295	1380	1.4×10^{28}	3.6×10^{37}

Table VI (continued)

Source	Distance Mpc.	P_{400} Watts/cps	Power Watts
3C 298	156	6.6×10^{25}	1.7×10^{35}
3C 310	162	8.4×10^{24}	2.2×10^{35}
3C 315	324	1.2×10^{26}	3.5×10^{35}
3C 317	105	2.9×10^{25}	7.5×10^{34}
3C 327	312	2.9×10^{26}	7.7×10^{35}
3C 338	91	1.8×10^{25}	4.8×10^{34}
Her A	465	4×10^{27}	1.0×10^{37}
3C 353	91	1.3×10^{26}	3.8×10^{35}
3C 382	171	4.6×10^{25}	1.3×10^{35}
3C 386	($\approx$10)	1.9×10^{23}	5.6×10^{33}
3C 388	273	1.3×10^{26}	3.8×10^{35}
Cyg A	168	1.5×10^{28}	4.8×10^{37}
3C 430	(35)	2.7×10^{23}	7.5×10^{33}
3C 433	306	3.5×10^{26}	9.7×10^{35}
3C 444	(400)	5.2×10^{26}	1.3×10^{36}
3C 442	243	7.6×10^{25}	2.0×10^{35}
3C 445	168	5.3×10^{25}	1.4×10^{35}
3C 452	246	2.2×10^{26}	6.0×10^{35}
23-112	246	4.7×10^{25}	1.2×10^{35}
3C 465	86	2.0×10^{25}	5.4×10^{34}

( ) Distance estimated from assumed absolute magnitude of -20.5. (15)

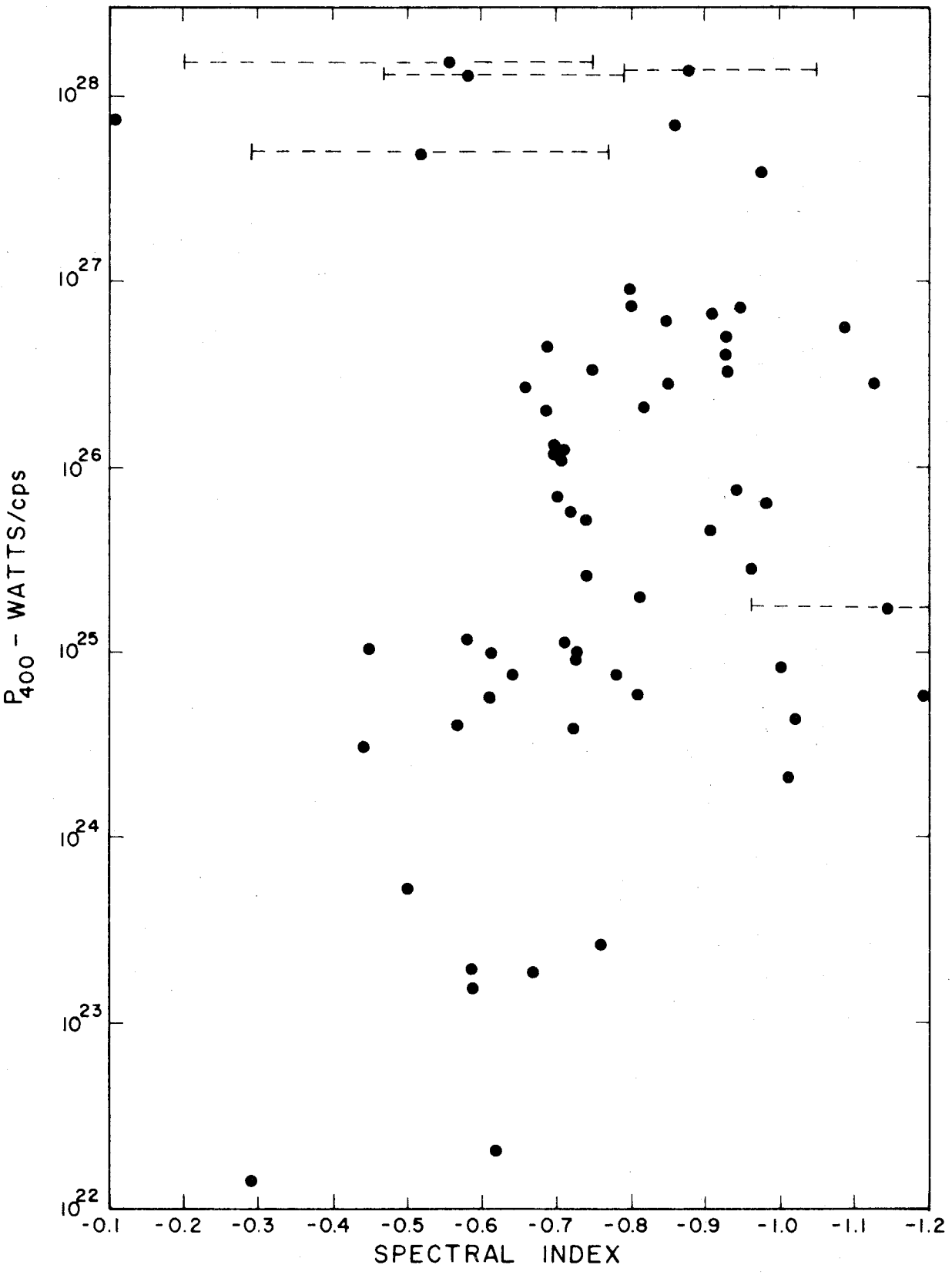

Figure 7 Relation between spectral index and monochromatic radiated power at 400 Mc.

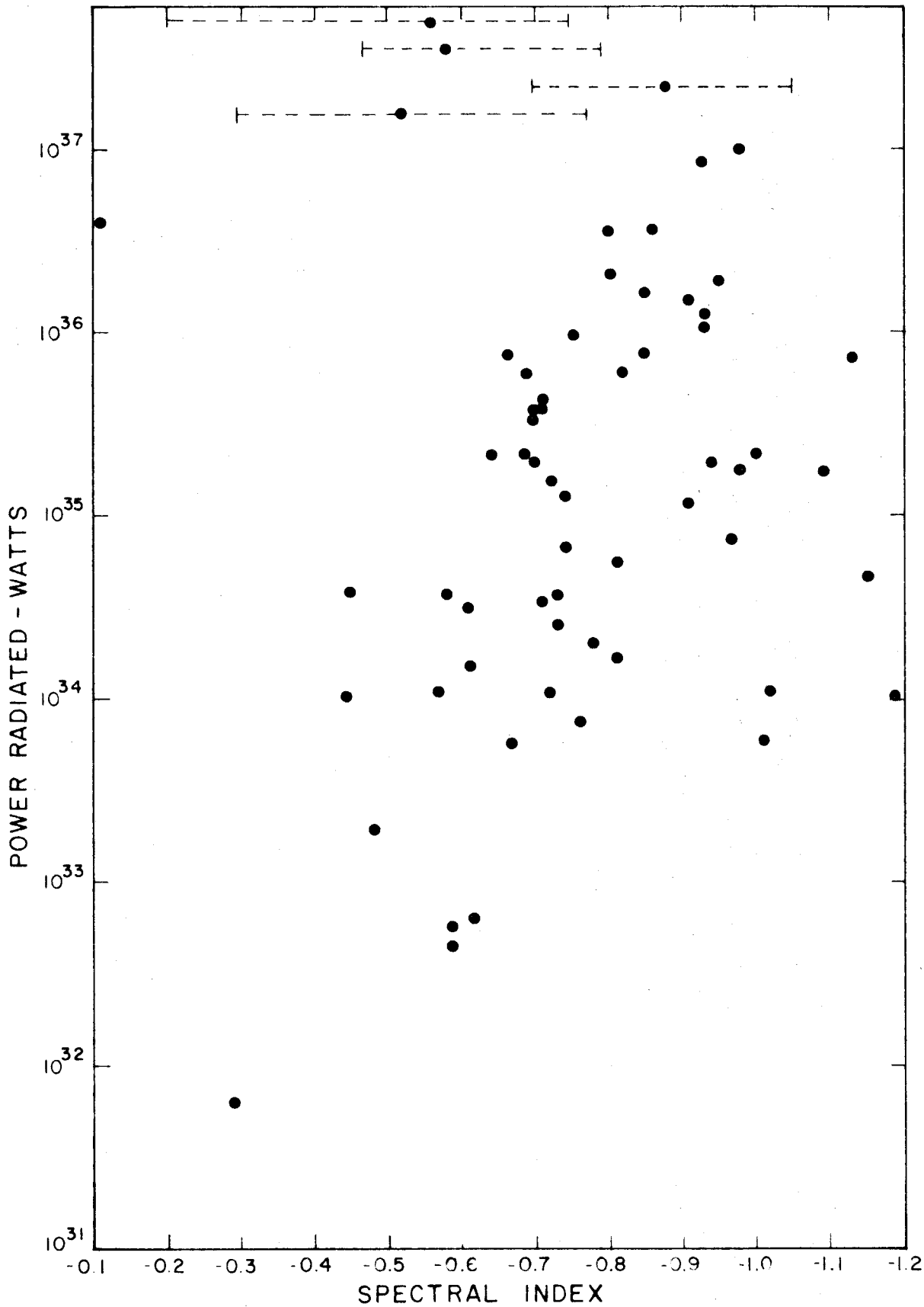

Figure 8 Relation between spectral index and total radiated power.

correlation exists between the spectral index and luminosity in the sense that the intrinsically weak sources generally have flat spectra. However, we note that for a given index there is a range of over two orders of magnitude in their luminosities.

If, in addition, we include in these plots the so-called "normal galaxies" whose radio emission is comparable with that of our own galaxy ($\approx 10^{31}$ watts), we find little, if any evidence for correlation between spectral index and luminosity. Although these sources have not generally been included in the present study*, Heeschen has found that their spectra are similar to that of the other non-thermal sources (39).

The indices of the most luminous sources, although not constant with frequency, tend to be considerably flatter than most sources. It is thus tempting to postulate that these are very young sources whose spectra are changing with time. Such an evolutionary scheme is outlined in Chapter V.

A similar comparison has been made between the spectral index and the spacial extent of the identified sources. Figure 9 shows a noticeable correlation between the index and the projected linear separation of the two components in the identified double sources. If confirmed, this result may provide a powerful method for estimating the distance to unidentified sources by measurements of the

---

*The sources NGC 253, NGC 1068, and M 82 should perhaps be included in this category.

Figure 9 Relation between spectral index and component separation.

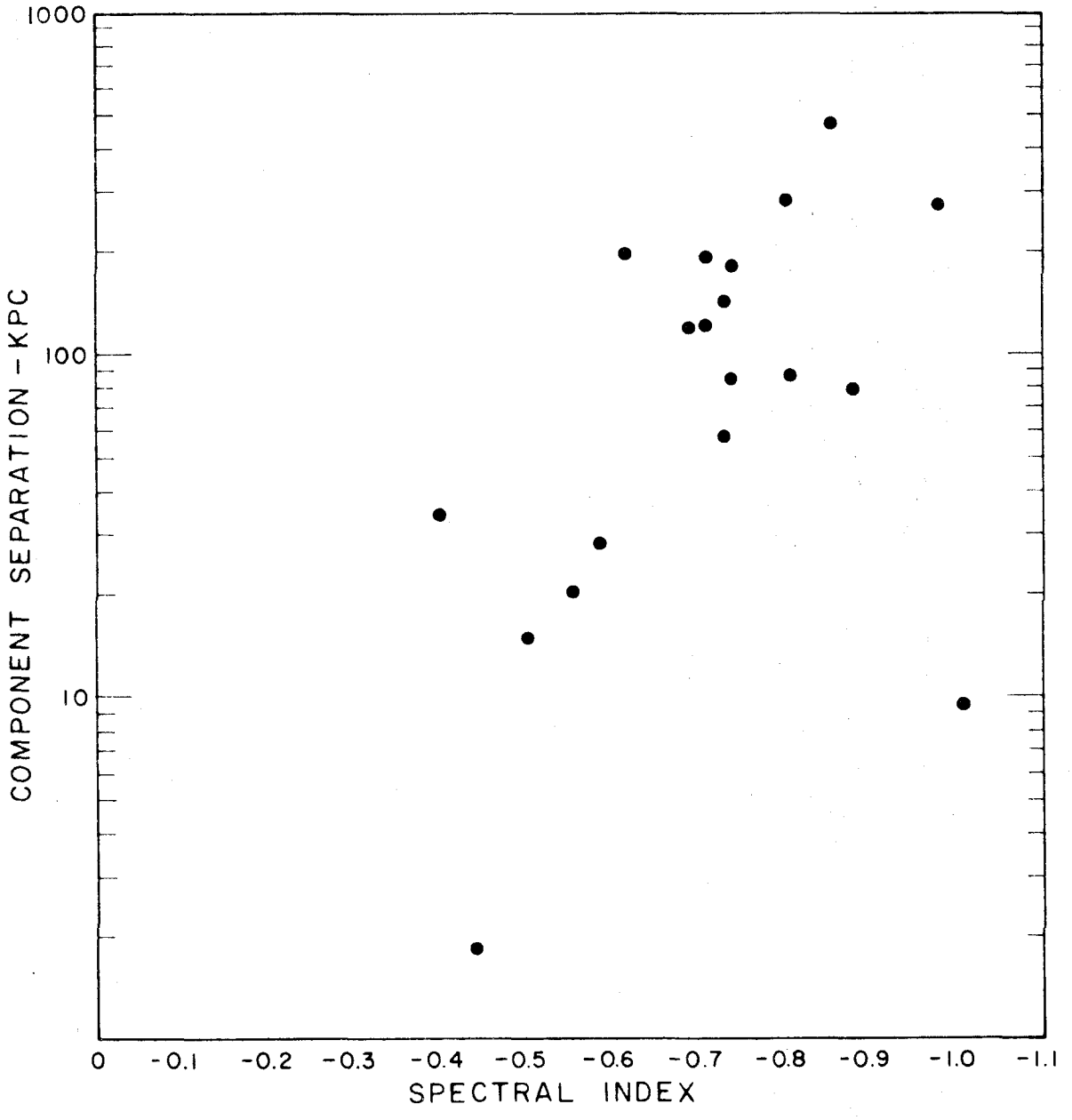

angular separation.

The indices for the non-thermal sources near the galactic plane have a considerably larger spread than the high latitude sources as shown by the histogram in Figure 6b. Among these sources, the identified supernova remnants appear to have constant indices out to very short wavelengths.

Observations at low galactic latitudes are hampered by high background temperatures and the large scale structure of many of these sources which often make it difficult to distinguish the limits of a discrete source from background irregularities. Furthermore, at low frequencies, the possibility of absorption in the interstellar medium cannot be neglected.

It is unlikely, however, that such instrumental effects alone can account for the large dispersion in the spectral index and it is felt that the class of sources found near the galactic plane does present more varied spectral indices than the extragalactic sources. Similar conclusions have been reached by Harris and Roberts on the basis of somewhat more limited data. A full discussion of these sources, which are presumed to be primarily remnants of old supernovae, has been given by Harris (5) and they are not treated further here.

Class C

On a logarithmic scale, the flux density of most of the sources in Class C decreases with increasing frequency

at a slowly increasing rate; that is, the spectral index becomes greater at the higher frequencies. In a few cases however, the reverse is true and the index becomes smaller at the high frequencies. Two of these sources, Perseus A and 3C 273, are known to consist of several components each with different spectral indices. Thus at low frequencies the major contribution to the flux density comes from the source with the steeper spectrum, and at high frequencies from the flatter one, giving a spectral index for the total flux density that slowly decreases with increasing frequency.

Several sources were found whose flux density slowly increases with frequency up to about 1000 Mc and then rapidly drops off above this frequency. Spectra of this type, which were previously unknown, have been designated as Class C_m and are discussed further below.

In order to quantitatively investigate changes in the spectral index with frequency, the index of each source was determined separately in the two frequency ranges 38 Mc to 475 Mc and 408 Mc to 3200 Mc. The difference between these two indices, which we have called the "curvature index", is tabulated in Table VII, along with the two values of the spectral index, for those sources where sufficient data exists.

An alternate approach would be to fit the data to a second degree expression in log f. The coefficient of the second order term would then represent a measure of the curvature of the spectrum. The present method was chosen

Table VII

Source	α_{low}	α_{high}	K
3C 10	- .65	- .62	.03±.10
00-210	+ .12*	- .91	1.03*
3C 18	- .53	- .97	.44±.17
3C 33	- .70	- .80	.10±.04
3C 48	- .29	- .77	.48±.08
3C 75	- .72	- .78	.06±.05
CTA 21	.18	- .52	.70±.13
3C 86	- .07	- .78	.71+
3C 119	- .02	- .65	.63±.10
3C 123	.71	- .80	.08±.03
05-36	.32	- .78	.46±.06
3C 147	- .20	- .75	.55±.15
3C 161	- .53	- .73	.20±.05
3C 196	- .69	- .86	.16±.05
Hydra A	.97	.97	.00±.04
3C 219	.72	.91	.19±.08
3C 237	.54	.74	.20±.15
3C 270	- .43	- .68	.25±.05
3C 273	- .53	- .30	-.23±.07
M 87	- .77	- .84	.07±.03
3C 283	- .63	1.10	.48±.11
NGC 5128	- .34	-1.03	.69±.20
3C 287	- .29	- .56	.27±.13
3C 295	- .47	- .79	.32±.07
3C 298	- .72	-1.22	.51±.10
3C 299	- .36	- .94	.58±.09
3C 317	- .74	-1.23	.49±.14
3C 338	- .96	-1.34	.39±.11
Her	-1.04	- .98	-.06±.06
3C 353	- .71	- .76	.05±.03
3C 380	- .77	- .71	-.05±.05
CTA 80	- .90	- .45	-.45±.14
3C 391	.49	-1.24	1.73
3C 433	- .66	- .90	.23±.06
3C 438	- .74	-1.05	.31 ±.08
3C 444	- .83	-1.15	.32±.10
CTA 102	.08	- .28	.37±.10
3C 452	- .83	- .78	-.05±.05

*Value depends on one questionable point at 85 Mc.

+Uncertain.

however, since the synchrotron mechanism predicts a spectral distribution whose asymtotic values can easily be interpreted in terms of the dominating energy loss mechanism in various energy ranges (Chapter 5). However, in general, the present data does not allow us to distinguish between these two analytical forms of the spectral distribution. It should be noted that where the frequency of maximum curvature differs significantly from 450 Mc, the two indices computed by this method are not necessarily equivalent to the actual values of the high and low frequency spectral indices.

Two sources, CTA 21 and CTA 102 present extreme examples of this class of spectrum. They both have spectra that are characterized by a slow increase in flux density up to about 1000 Mc and a rapid drop off above this frequency. These sources represent a previously unknown type of spectral distribution for non-thermal radio sources. Because of the uniqueness of the spectra, the original records at all frequencies were carefully reinspected for any possible misinterpretation. No such evidence was found.

Both of these sources are located well away from the galactic plane and have angular diameters less than 1' of arc (23). As the plates of the Palomar Sky Survey show no evidence for optical radiation or obscuration in the vicinity of either source it seems unlikely that the observed spectrum can be explained by thermal radiation or absorption in an ionized region.

One other source, MSH 00-210, may also be of this

type. The present Caltech measurements alone do not show any evidence for a maximum in the flux density and the tentative classification is based solely on the 85 Mc measurement. However, Mills, Slee, and Hill have listed this source as "extended" (21) indicating that some or all of the measurements may be effected by resolution or confusion with a nearby source. Therefore until the 85 Mc measurement is confirmed, the classification of this source must be regarded as questionable.

In addition to CTA 21 and CTA 102 there are a number of Class C sources whose high frequency indices lie in the same range as the Class S sources (-0.6 to -0.9), while the low frequency index is considerably smaller (0.0 to 0.5). These have been designated Class C_L. Several of these objects, 3C 48, 3C 147, 3C 286, and 3C 295, are believed to be at very great distances (40),(41),(42) and are among the most powerful radio sources known. The former three, along with 3C 273 and 3C 196, have been tentatively identified with peculiar objects which although thought to be distant galaxies, optically present a stellar image on direct photographs (42),(43).

The remaining sources with this type of radio spectrum, which have not yet been optically identified are generally found to have an extremely high surface brightness. As accurate values for both the curvature index and brightness temperature are difficult to obtain for individual sources, we have calculated the mean curvature index in decade intervals of brightness

temperature. In this application, the term brightness temperature refers to the mean temperature of the principle component(s). These have been estimated with the help of Dr. L. R. Allen, using all available data on the brightness distribution of extragalactic sources.

Figures 5 and 6 show a distinct tendency for the curvature to increase with increasing surface brightness. As a high surface brightness implies the presence of a strong magnetic field, it seems likely that the observed curvature of the spectra can be explained as a result of the more rapid loss of energy of the high energy electrons, due to synchrotron radiation, as the source evolves. This result, as well as the relation between spectral index and component separation in the double sources, supports our tentative evolutionary hypothesis above and is discussed further in Capter V.

Sources whose spectra are "normal" at low frequencies and become unusually steep at high frequencies have been designated as Class C_H.

Class T

The nature of these sources is well understood in terms of free-free transitions in HII regions with electron temperatures of about 10,000°K (44). At low frequencies where the source is optically thick, the spectral distribution of the radiation is given simply by the Planck formula for black body radiation. The spectral index, α, is then

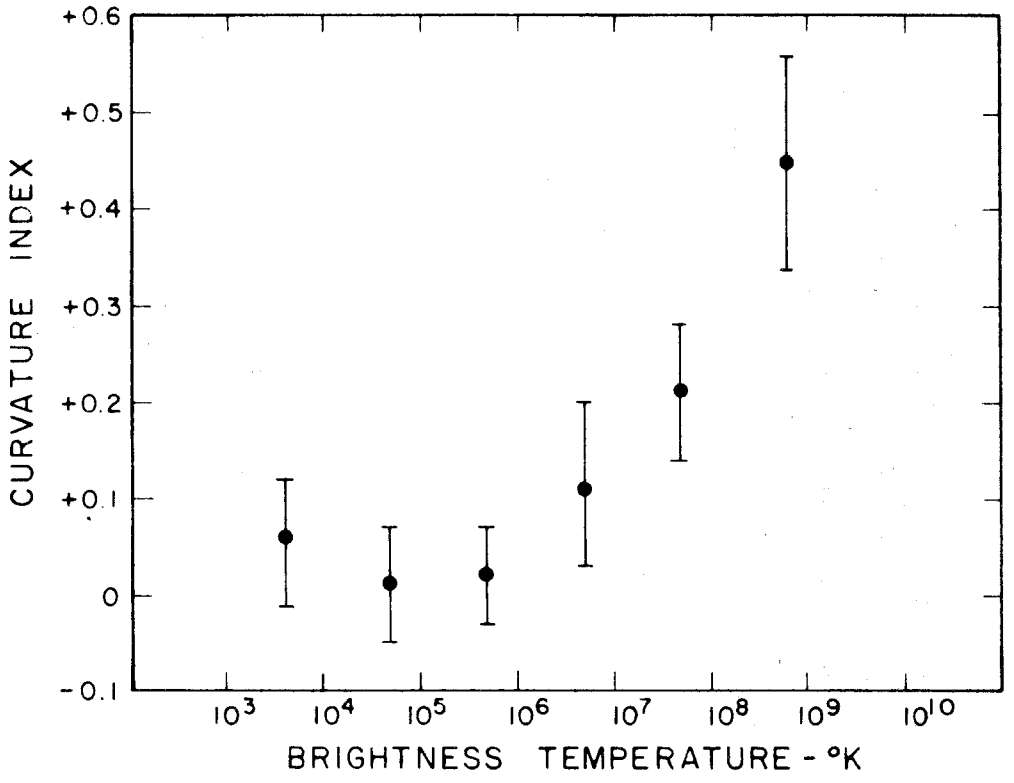

Figure 10 a) Curvature index vs. surface brightness.

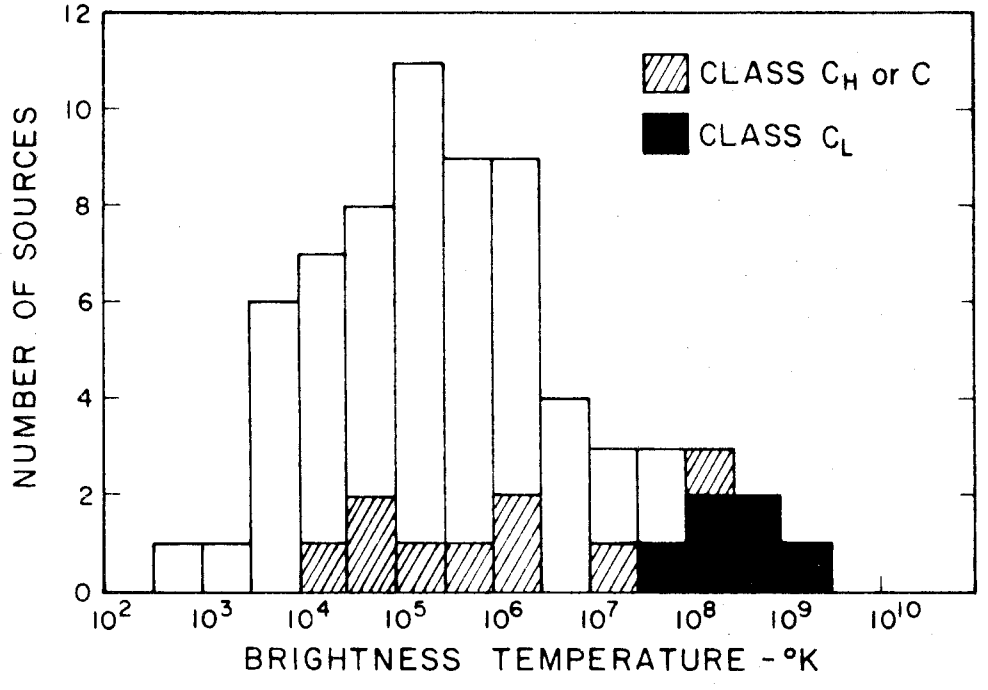

Figure 10 b) Histogram showing relation between spectral class and surface brightness.

equal to +2.0. The optical depth which varies approximately as (frequency)$^{-2.1}$ becomes small at high frequencies and the spectral index is then about -0.1. The observed spectra closely follow this expected distribution. Due to the rapid decrease in brightness with decreasing frequency, these emission nebulae are observed in absorption at sufficiently low frequencies where the surface brightness becomes less than that of the galactic background (44). As these sources have been discussed by many workers, and since the emission mechanism is reasonably well understood, they are not treated further here.

4.2 Selection Effects

As most of the sources described previously were selected from the stronger sources in the low frequency catalogues, there may be some tendency to discriminate against sources with very flat spectra. In fact, three sources (CTA 21, CTA 26, and CTA 102) first discovered by chance at 960 Mc while other sources in the region were being studied (4), were subsequently found to have extremely flat spectra. This suggests the possible existence of a class of source that might most easily be detected at decimeter wavelengths. Sources in the southern part of the sky are less subject to such effects as these were chosen from a systematic study at 960 Mc down to a relatively low level of flux density (45) of sources in the Sydney 85 Mc catalogue (20),(21).

Likewise, there may be some discrimination against sources with very steep spectra which may be too weak to be observed at high frequencies. It must be emphasized that the mere inability to detect a source which appears in a low frequency catalogue, at decimeter wavelengths, is not alone evidence that the source has an unusually steep spectrum, unless its existence is verified by observations with several dissimilar instruments.

Since at the present time there are no published systematic surveys made at decimeter wavelengths of the region of the sky away from the galactic plane, it is not possible to exclude these selection effects from spectral studies. In order to estimate the magntiude of these effects, the Caltech interferometer has been used to survey the region of the sky between $23^{\circ}50'$ and $30^{\circ}10'$ at a frequency of 1421 Mc.

The survey was performed with an east-west baseline of 200 feet (290λ) corresponding to a fringe spacing of 12'. Both dishes were pointed toward the meridian, allowing the sources to drift through the primary beam pattern. Each day the antennas were moved 20' in declination. All sources detected in the survey were then examined in more detail at an antenna spacing of 100 feet (24' fringe spacing). The apparent position of each source was first measured in the coordinate system of the telescope and then the antennas were made to track on that position for several interference fringes to determine the source intensity.

Altogether 146 sources were detected, of which 115 were located more than 10^{o} from the galactic plane. This corresponds to about one source per seventy beam widths; thus the effects of confusion are felt to be small.

All 27 of the sources listed in the Revised 3C catalogue (18) in the region of the sky covered by the survey were detected, and the observed flux densities have been used to determine their spectral index between 178 Mc and 1421 Mc. It was found that one-half of the sources at high galactic latitudes have a spectral index in the range -0.81 ± 0.1.

As the remaining 119 sources have not been previously catalogued, we cannot determine their individual spectra. However, the relation between the distribution of the number of sources with respect to flux density at two different frequencies will depend on the spectra of the sources, and thus a comparison of the number-flux-relation at 1421 Mc and some other frequency will provide an indirect measure of the distribution of spectral indices. The dependence of the number-flux-relation on frequency can be determined as follows.

Let the number of sources, N(S) at some frequency f_1 greater than S be given by (14)

$$N_1(S) = K_1 S_1^{x} \quad . \tag{4.6}$$

Then for sources with a spectral index α, we have at some frequency f_2

$$N_2(S) = N_1(S) \left(\frac{f_2}{f_1}\right)^{-\alpha x} \tag{4.7}$$

and if $P(\alpha)d\alpha$ is the normalized probability of finding a source with a spectral index between α and $\alpha+d\alpha$

$$N(S_2) = N(S_1) \int_{-\infty}^{\infty} \left(\frac{f_2}{f_1}\right)^{-\alpha x} P(\alpha)d\alpha \equiv N(S_1)\ T\ (x,\alpha)\ . \quad (4.8)$$

Finally, if $P(\alpha)$ is given by a Gaussian with a mean value α_o and dispersion σ,

$$N(S_2) = \frac{N(S_1)}{\sqrt{2\pi}\sigma} \int_{-\infty}^{\infty} \left(\frac{f_2}{f_1}\right)^{-\alpha x} e^{-(\alpha-\alpha_o)2/2\sigma^2}\ d\alpha\ . \quad (4.9)$$

Performing the integral we find

$$N(S_2) = N(S_1) \left(\frac{f_2}{f_1}\right)^{-\alpha_o x}\ e^{\frac{1}{2}\sigma^2 x^2 \nu^2}$$

where $\nu = \ln f_2/f_1$. (4.10)

Using our earlier results for the distribution of spectral indices at high galactic latitudes for $P(\alpha)$ along with the 178 Mc source counts, equation 4.9 was numerically integrated to determine the expected form of the number-flux-relation at 1420 Mc. This indicated about a 20 per cent deficiency in the observed number of sources, which in view of the large experimental uncertainties cannot be regarded as significant. The best fit to our data gives a value of $x_{1420} = -1.76$ and $K_{1420} = 138$.

The general agreement of the two surveys indicates that statistical inferences derived from the observed spectra cannot be significantly effected by observational selection.

This of course does not imply that the observed distribution of spectral indices is independent of frequency. Clearly as we go to higher frequencies there will be a tendency to observe the sources with the flat spectra. This is a direct result of the number-flux-relation which as the frequency is raised will cause more sources with flat spectra to rise above a given flux limit than sources with steep spectra to fall below this limit.

To find the relation between the observed distribution of spectral indices at two frequencies, we make use of equation 4.9. Let $P(\alpha)$ and $Q(\alpha)$ be the normalized distribution of spectral indices at frequencies 1 and 2 respectively. Thus,

$$\int_{-\infty}^{\infty} P(\alpha)\,d\alpha = 1 \qquad \int_{-\infty}^{\infty} Q(\alpha)\,d\alpha = 1 \quad .$$

Interchanging the subscripts on equation 4.9, we have

$$N(S_1) = \frac{N(S_2)}{\sqrt{2\pi\sigma}} \int_{-\infty}^{\infty} \left(\frac{f_1}{f_2}\right)^{-\mu x} Q(\mu)\,d\mu \qquad (4.11)$$

where μ is a dummy index of integration. Putting this back into 4.9 we find

$$\int_{-\infty}^{\infty} \left(\frac{f_2}{f_1}\right)^{-\alpha x} P(\alpha)\,d\alpha \int_{-\infty}^{\infty} \left(\frac{f_2}{f_1}\right)^{\mu x} Q(\mu)\,d\mu = 1 \quad . \qquad (4.12)$$

This merely states the transformation from f_1 to f_2 and back again to f_1 must be identically equal to unity. The solution of this singular integral equation is

$$Q(\alpha) = A \left[\frac{f_2}{f_1}\right]^{-\alpha x} P(\alpha) \qquad (4.13)$$

where A is chosen so that

$$\int_{-\infty}^{\infty} Q(\alpha)d\alpha = 1 \quad . \qquad (4.14)$$

Thus, if $P(\alpha)$ is the known distribution of indices for the N brightest sources at f_1 , then the distribution of indices of the N brightest sources at f_2 is given by equation 4.13. These, of course, are not the same N sources that were observed at f_1 .

In the special case where $P(\alpha)$ is a Gaussian with a dispersion σ , $Q(\alpha)$ is also a Gaussian with the same dispersion but with the mean value displaced by the amount $x\sigma^2 \ln(f_1/f_2)$.

4.3 Integrated Fluxes

The observed spectral distribution of the flux density has been used to estimate the integrated flux of each source. With but a few exceptions, observations are not available below 38 Mc or above 3000 Mc and it is therefore necessary to make some assumptions about the spectral dependence outside the observed frequency range. We have assumed lower and upper cutoff frequencies of 10 Mc and 10,000 Mc respectively, which are consistent with the present data. Expression 4.4 was integrated between the two cutoff frequencies to determine the total flux, F. Except in a

few cases where data was available outside the frequency range 30 to 3000 Mc, the spectral index was generally assumed to be 0.0 between 10 and 30 Mc, and -1.0 between 3000 and 10,000 Mc. Until data becomes available over a wider range of frequencies, the present calculations must be regarded as only order of magnitude estimates. Values of the integrated flux, F, are given in column 6 of Table V.

As the number of radio sources identified with optically observable objects is rapidly increasing, it is now possible to determine the distance and thus the absolute luminosity and linear dimensions for a large number of sources. Columns 3 and 4 of Table VI give the absolute monochromatic luminosity at 400 Mc and the total power radiated for all sources whose distances are known. The distances to the sources were obtained from the list compiled by Maltby, Matthews, and Moffet (48), or from redshifts provided by Schmidt (49).

The following expressions were used in making these calculations (see following section).

$$P_f = \frac{4\pi}{c^2 H^2} \frac{z^2}{(1+z)^{1+\alpha}} S_f \qquad (4.15)$$

$$P = \frac{4\pi}{c^2 H^2} z^2 F \qquad (4.16)$$

where P_f is the power radiated per unit bandwidth at a frequency f, S_f the observed flux density at the same

frequency, P the total radiated power, F the integrated flux, and z the value of the red shift $\Delta\lambda/\lambda$. The Hubble constant, H, has been taken equal to 100 km/sec/Mpc (46). These formulae are exact for world models with $q_o = +1$ and approximately correct for other models when $z<<1$. The latest observational data give $q_o = +1 \pm 1/2$ (47). This particular choice of world models is fortuitous in that the various effects of the redshift cancel out in equation 4.16, and due to the nature of the spectral law, nearly do so in equation 4.15, i.e. $1+\alpha \approx 0$.

4.4 Effect of the Redshift

As many of the sources reported here are believed to be at great distances, it is of interest to examine the effect of the redshift of the observed spectra.

We let $P(f')$ be the spectral dependence of the radiation at the source, z, $\Delta\lambda/\lambda$ the value of the redshift, f the observing frequency, and $f' = f(1+z)$ the frequency of emission. Then the flux density observed at the earth is given by

$$S_f = \frac{P\left[f(1+z)\right](1+z)}{4\pi D^2(z)} \quad , \qquad (4.17)$$

where $D(z)$ is an appropriately defined luminosity distance equal to (92)

$$D(z) = \frac{cz}{H}\left\{1 + \frac{1}{2}(1-q_o)z+....\right\} \qquad (4.18)$$

the value of the deceleration parameter q_o depending on the particular choice of world models.

The spectral dependence of the flux density observed at a frequency f thus corresponds to the spectral dependence of emission at a frequency $f' = f(1+z)$.

In the case where $P(f') = P_o f^{\alpha}$ and α is constant, equation 4.17 becomes

$$S(f) = \frac{P_o f^{\alpha}(1+z)^{1+\alpha}}{4\pi D^2(z)} \quad . \qquad (4.19)$$

So the observed index is equal to the index of emission. If however, α is a function of frequency, the observed spectral index will clearly depend on the value of z.

Since many sources do show a variation of the spectral index with frequency, this raises the interesting possibility of obtaining radio redshifts from spectral observations. However, it is shown in Chapter V that the index of the older sources are not expected to vary with frequency below some upper cutoff frequency and that evolutionary effects will probably cause significant changes in the spectra of the young sources in a time short compared to the cosmological time scale.

Although we are thus unlikely to find any unique relation between the redshift and observed spectral characteristics, the possibility remains that when we better understand the nature of strong radio galaxies we may be able to predict the form of the spectrum from some other

observed property of the source such as its brightness temperature or polarization, and by comparing this with the observed spectrum obtain an estimate of the redshift. At the present time however, we must regard as premature any attempts to determine the redshift of individual sources from observations of their spectra.

An alternate approach is to make a statistical analysis of the observational data. As has been pointed out by Conway, Shakeshaft, and Whitfield, the tendency for spectra to steepen at high frequencies will cause the fainter sources, which are presumed to be on the average more distant, to have steeper observed spectra due to their large redshifts (50). Such an effect has been reported by Whitfield (51) and by Kellermann and Harris (45), although the latter attributed this to progressively increasing uncertainties in the positions of the weaker sources, thus causing the measured flux density to be less than the true value. More recent work by the author tends to support these original conclusions. In a more limited study of radio spectra, Goldstein finds no evidence for such an effect and attributes Whitfield's results to the effects of confusion and resolution (33).

The present data has been carefully investigated for any systematic change in the apparent spectral index with flux density. In order to avoid the selection effects discussed earlier, the spectral indices were compared with

the measured flux densities at 178 Mc which were taken from a systematic survey of the sky.

The results, which are shown below, indicate that the spectral index is essentially independent of the observed flux density.

Table VIII

S*	mean α
>50	.78 ± .03
32 - 50	.76 ± .02
25 - 32	.80 ± .02
21 - 25	.75 ± .02
16 - 21	.71 ± .04
14 - 16	.72 ± .03
<14	.83 ± .04

*Units of $10^{-26} w/m^2/cps$

An interesting consequence of curved spectra is that if the majority of observed sources lie at cosmologically significant distances, counts of sources made at high frequencies will indicate a relative deficiency of weak sources over counts made at low frequencies. Although this is clearly related to the apparent change in the spectral index with the observed flux density, current techniques are now making available statistical data in the number-flux-relation down to a very low level of flux density where cosmological

effects may become important (14), but where studies of individual sources are not yet possible. Comparison of high sensitivity surveys made at widely spaced frequencies thus offers a powerful technique for investigating the distribution of radio sources in space, and could provide a test to distinguish between various cosmological models.

5.4 Changes in Brightness Distribution with Frequency

Brightness distributions of a number of sources are now available over a range of frequencies. Comparison of interferometer measurements at 159, 960, and 1420 Mc indicates that there is little evidence that the structure of these sources is frequency dependent (24).

In a few notable exceptions, particularly sources with a core-halo type structure, it appears that the two major components have distinctly different spectra. A few of these sources are discussed below in some detail.

Perseus A

Observations by Miss Leslie and Elsemore at Cambridge (52) at 178 Mc have shown this source to consist of three major components. Two are small diameter objects having a ratio of flux densities of about 2.5 to 1. The stronger of these, 3C 84 appears to be associated with the galaxy NGC 1275 (53) and the weaker, 3C 83.1 with NGC 1265 (52), although the latter identification must still be regarded as tentative. The third component is 26' of arc in diameter and has a flux density approximately equal to

3C 84 at 178 Mc. From considerations of its size and intensity, Miss Leslie and Elsemore have shown that it is unlikely that the extended source is due to the integrated emission from the Perseus cluster of galaxies.

More recent observations by Lynds and Sobieski at 3000 Mc have also isolated the two small diameter sources, but find no evidence for the extended component (54). From a comparison of flux density measurements made by many workers, they conclude that the spectral index of the source Perseus A is quite large at low frequencies and becomes smaller at decimeter wavelengths.

Because of this peculiar spectrum and the complex nature of the source, we have attempted to obtain the spectrum of each of the three components separately.

The two measurements of the weaker sources at 178 and 3000 Mc have been used to determine its spectral index. From this, the expected flux density of this component was computed at 475, 710, 958, 1420, and 2840 Mc, and this was subtracted in the proper phase from the observed interferometer amplitude to determine the flux density of the stronger component. We have then taken all the available measurements of the total flux density of Perseus A and subtracted off the contribution of the "point" sources. The remainder is assumed to be due to the extended source. The results are consistent with a spectral index of -.57 and -.62 for 3C 83.1 and 3C 84 respectively. The extended source, on the other hand, appears to have an index of about -1.25, placing

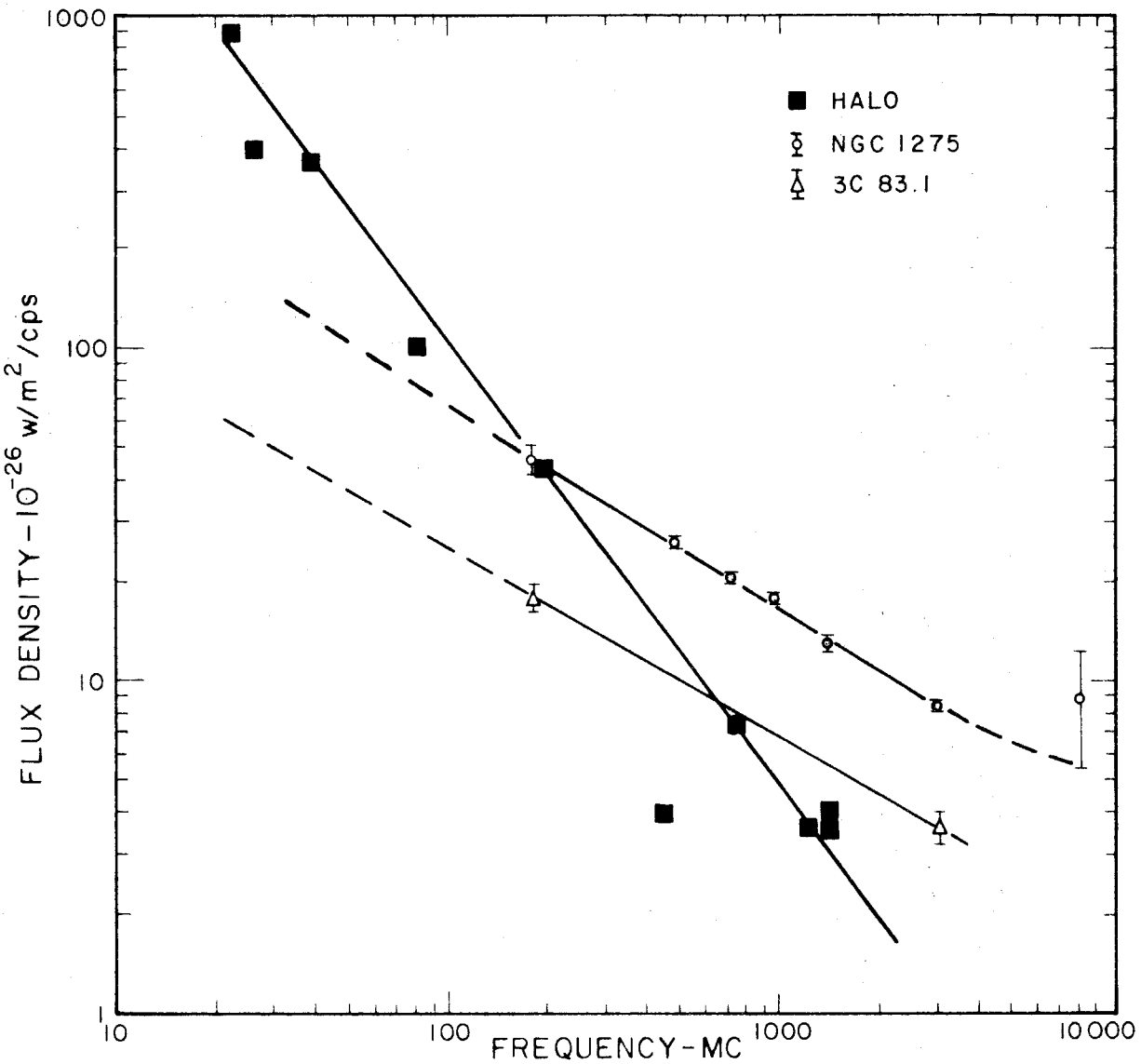

Figure 11 Spectrum of Perseus A.

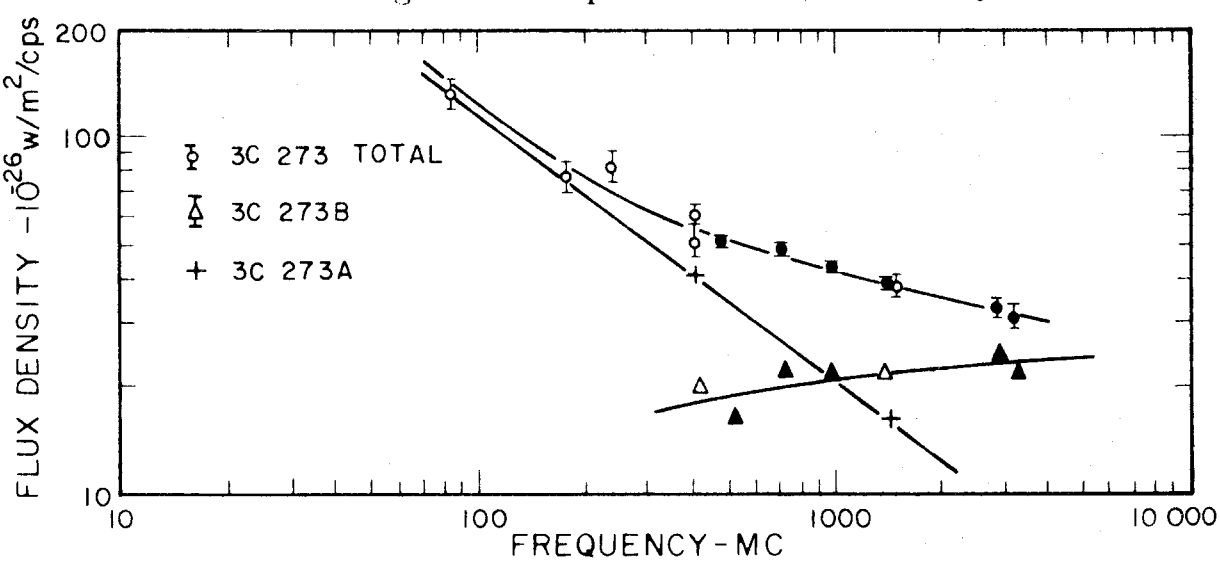

Figure 12 Spectrum of 3C 273.

it among the steepest known spectra, although the Green Bank measurement at 440 Mc is inconsistent with this interpretation. The spectrum of the three components of Perseus A is shown in Figure 11.

3C 273

3C 273 is one of the few Class C sources whose spectral index decreases with increasing frequency. Recent observations of this source at several frequencies during a series of lunar occultations suggest that this source consists of two components with different spectral indices (55).

Using the ratio of flux densities of the two components found from the occultation measurements along with other measurements of the total flux density, we have attempted to construct the spectra of the individual components. As these authors have pointed out, the spectrum of one component is typical of extragalactic radio sources in general, while the other is extremely flat. If we assume that the index of the "normal" source of -0.76 between 410 and 1420 Mc remains constant over the range 85 to 3200 Mc, then the contribution of this source can be subtracted from the measurements of the total radiation to determine the spectrum of the other source. The result of this procedure shown in Figure 12 indicates a spectrum somewhat similar to CTA 21 and CTA 102.

Alternately, of course, we can allow the index of both components to vary with frequency; but until more data

is available it seems pointless to speculate on more complicated models, and for the present we must regard these results as tentative.

Furthermore, since the authors make no mention of the relative orientation of the antenna feeds, we cannot neglect the possiblity that one or both of the components is strongly polarized, thus giving spurious results in the measured relative strength of the two components. In this respect, we note that the integrated emission from 3C 273 is known to be a few per cent linearly polarized (31),(32).

Virgo A (M 87)

Interferometric measurements over a wide range of frequencies has shown that, at least at decimeter wavelengths, this source consists of a small core of less than 1' of arc in diameter and an extended halo. From a comparison of visibility functions measured at several frequencies, Moffet has shown that the relative intensity of the core increases with increasing frequency (56). Since that time, additional measurements of M 87 have become available and it is now possible to construct somewhat more detailed spectra of the individual components.

Interferometric measurements at 85 (57), 101 (58), 159 (23), 960 (8), 1420 (59), and 2840 Mc were used to determine the flux density of the core at each of these frequencies. These were then subtracted from the total flux density to determine the flux density of the halo. This

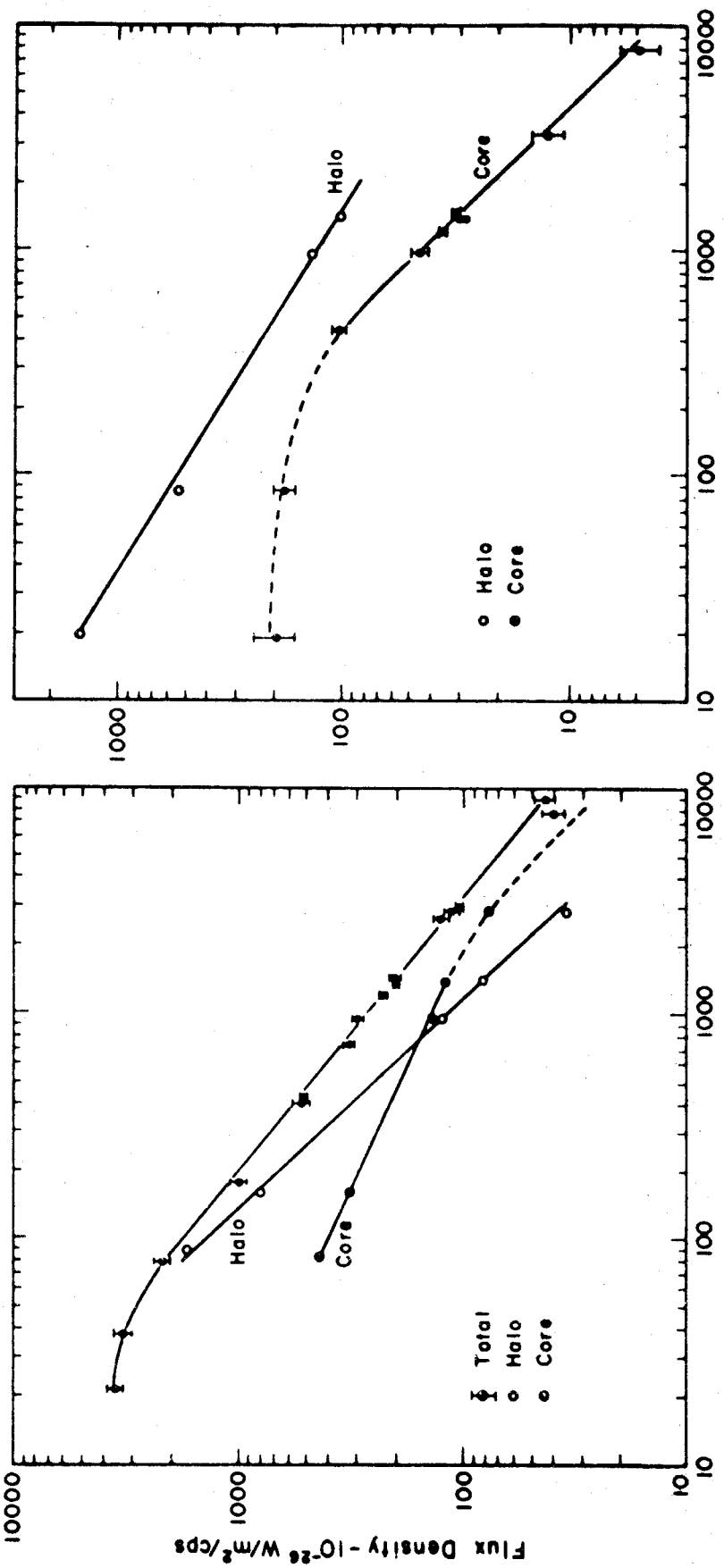

Figure 13 Spectrum of M 87

Figure 14 Spectrum of NGC 5128

procedure gave an index of -0.44 and -1.02 for the core and halo respectively. As shown in Figure 13, the total flux density measured at 22 Mc and 38 Mc indicates that the index of the halo must decrease below 85 Mc. Likewise, the 2840 Mc value for the core, along with the 8,000 and 9,000 Mc total flux density measurements, suggests that the index of the core increases above 1500 Mc.

This conclusion is supported by optical measurements of the "jet" in M 87 at 4,350 and 6,300 A^o by Bless (60). If we accept the association of the optical "jet" with the radio core, then it is reasonable to assume that the continuous optical spectrum in the jet is due to synchrotron radiation as proposed by Burbidge (61) and Shklofsky (62). The measured flux density at 6,300 A^o is in good agreement with the extrapolation of the high frequency part of the radio spectrum of the core (α=-0.65).

It should be noted that, because of uncertainties in the measured radio position of the core, its identification with the optical jet cannot be regarded as certain. The position angle of the major axis of the core does however lie along the direction of the jet(59).

Centaurus A (NGC 5128)

The source Centaurus A has been observed from 19.7 to 8,000 Mc by a large number of observers.

It has been known for some time that this source

consists of two components - an extended region of low surface brightness covering some 20 square degrees of the sky (63),(64),(65),(66); plus a smaller double source more or less symmetrically placed with respect to the parent galaxy NGC 5128 (67). As the extended and central components are easily separated with pencil beam antennas of moderate resolution, we are able to obtain the spectrum of the two components individually.

The data are consistent with a spectral index of -1.03 for the central component above 400 Mc and a considerably smaller value below this frequency. The extended region, on the other hand, appears to have a constant spectral index over the observed frequency range from 19.7 to 1400 Mc. Unfortunately, due to its low surface brightness at high frequencies, there are no published flux densities of the halo above 1400 Mc.

In view of the large degree of polarization recently found both in the central and extended sources, these results must be regarded with some caution. In particular, the central source itself has now been resolved at a number of frequencies into two smaller components (67), (68), each of which is considerably polarized (69) thus complicating any comparison of the brightness distribution of this source at different frequencies.

4.6 Extension of the Spectra to Optical Frequencies

Measurements are now available for several sources

which indicate that at least part of the observed optical and infrared radiation is due to synchrotron radiation. Perhaps the best known of these is the Crab Nebula, where the synchrotron mechanism provides the only satisfactory explanation of the strong continuous radiation at optical frequencies (70). O'Dell has recently summarized measurements of the flux density of this source at optical and infrared wavelengths. He found that the radio spectrum continues essentially unchanged out to about 10^{14} cps, and that beyond this frequency the flux density rapidly decreases (71). As shown in the following chapter, this is the form of the spectrum expected if there is a sharp cutoff in the relativistic electron spectrum.

Matthews and Sandage (42) have shown that the optical radiation from the "stellar" type objects associated with the sources 3C 48 and 3C 196 may be due to synchrotron radiation with upper cutoff frequencies of 7×10^{14} and 5×10^{14} cps respectively. More recently, Oke (72) has obtained infrared and optical measurements of the flux density of 3C 273B using a photoelectric scanner. He finds, that in addition to a black body spectrum between 3300 and 8400 A, the flux density rapidly increases above 8400 A and suggests that at least part of the infrared continuum is due to synchrotron radiation.

V. PHYSICAL PROCESSES IN EXTRAGALACTIC SOURCES

The suggestion that synchrotron radiation was responsible for non-thermal cosmic radio emission was first put forward by Alfven and Herlofson (73) and Kiepenheuer(74) in 1950. Their predictions were based on the work of Schwinger(75) and Vladimerski (76) who developed the fundamental theory of the radiation from an ultrarelativistic electron spiraling in a weak magnetic field. This theory was then applied to astrophysical conditions by Shklovsky (84), Ginzburg (85), and other Soviet workers during the early 1950's. Their work however, received little attention outside the Soviet Union until 1954 when Oort and Walraven confirmed Ginzburg's prediction of polarization of the optical radiation from the Crab Nebula (70).

Finally, the discovery in 1962 that the radio emission from a large number of galactic and extragalactic sources as well as from the galactic background was partially linearly polarized (30),(31),(32),(69) removed one of the major obstacles to the general acceptance of the synchrotron theory. The rest of this section is therefore devoted to interpreting the spectral data in terms of this mechanism.

In this treatment we shall neglect the possible effects of absorption in an ionized medium between the source and observer. This should not be important at frequencies above 40 Mc. Although the sharp cutoff in the spectrum of

Cygnus A and Cass A below 30 Mc is probably due to absorption from free-free transitions in galactic HII regions, we note that the various observed forms of the spectra above 38 Mc are not consistent with a simple absorption theory. While Greenstein and Minkowski (77) and Roman and Haddock (78) have succeeded in producing a variety of spectra by constructing models consisting of a non-thermal source in or behind a region of varying size and optical depth, their models are rather arbitrary and involve the adjustment of a relatively large number of parameters to fit the observed spectra.

Although Greenstein has found from a study of optical emission lines that regions of very high density are associated with some of the extragalactic sources (79), it is clear for several reasons that these regions cannot be physically coincident with the source of synchrotron radiation. If this were the case, Faraday rotation of the plane of polarization would be quite large. However, Seielstad has found that there is little if any Faraday rotation within the extragalactic sources (69). Furthermore, as pointed out by Greenstein, at these densities the ionized region would be opaque to the synchrotron radiation (79).

The problem of stimulated emission by free-free transitions and its effect on the spectral distribution of the radiation has been the subject of a number of recent papers. Twiss has shown that the net absorption coefficient for free-free transitions will always be positive (80),(81).

However, Browne has disagreed with this conclusion and finds that under certain conditions there will be negative absorption and the medium will act as an amplifier (82),(83). Clearly, further studies on this mechanism as well as stimulated emission from free-bound transitions are needed before any definite conclusions can be reached.

Twiss has also considered the possibility of absorption by relativistic electrons and finds that this can become important only at frequencies below about 10 Mc (80).

5.1 Basic Synchrotron Theory

The well known equation for the radiation, at a frequency ν, of a single electron moving in a uniform magnetic field can be written as (70)

$$P(\nu,E,\theta) = CH_{\perp}\xi\ F(\xi) \quad , \tag{5.1}$$

where ν_c is the critical frequency defined by

$$\nu_c = \frac{3c}{4\pi mc} H_{\perp} \left(\frac{E}{mc^2}\right)^2 = L\ H_{\perp}\ E^2 \quad , \tag{5.2}$$

and where

$$F(\xi) = \int_{\xi}^{\infty} K_{5/3}(\eta)d\eta \quad . \tag{5.3}$$

In these expressions, $H_{\perp} = H\sin\theta$, $K_{5/3}(\eta)$ is a modified Bessel function of the second kind, θ is the angle between the velocity and the magnetic field, E is the electron

energy, and $\xi = \frac{\nu}{\nu_c}$. When H is in Gauss, E is in Bev, and m and c in cgs units, then

$$C = 2.343 \times 10^{-22} \quad \text{and}$$

$$L = 1.608 \times 10^{13} \quad .$$

The radiation is highly concentrated along the direction of the instantaneous velocity with an angular width of the order mc^2/E. It is elliptically polarized with the polarization ellipse having an axial ratio of 7 to 1. The orientation of the ellipse is such that seven times as much energy is radiated with the electric vector parallel to the plane of the orbit as with it perpendicular.

Each electron radiates energy at the rate (70)

$$\frac{dE}{dt} = -\frac{2e^4}{3m^2c^3} H_\perp^2 \left(\frac{E}{mc^2}\right) = -A H_\perp^2 E^2 \text{ ev/sec} \quad (5.4)$$

where $A = 3.793 \times 10^{-6}$.

The solution of equation 5.4 for a single electron in a uniform magnetic field is

$$E = \frac{E_o}{1+A H_\perp^2 E_o t} \quad (5.5)$$

where E_o is the initial energy of the electron. Thus, the time in which the energy will decrease to 1/2 of the initial energy is

$$t_{1/2} = \frac{1}{AH_\perp^2 E_o} = \frac{8.35}{H_\perp^2 E_o} \times 10^{-3} \text{ years.} \quad (5.6)$$

We now consider the spectral distribution of the radiation from a collection of electrons with an energy distribution N(E) between E_1 and E_2 .

Expression 5.1 becomes

$$P(\nu,\theta) = \frac{1}{2}CL^{-1/2}H_{\perp}^{2}\nu^{1/2}\int_{\xi_1}^{\xi_2}\xi^{-3/2}N(\xi)F(\xi)d\xi \qquad (5.7)$$

where ξ_1 and ξ_2 are given by

$$\xi_1 = \nu/\nu_1 \qquad \xi_2 = \nu/\nu_2$$

where ν_1 and ν_2 are the critical frequencies corresponding to E_1 and E_2.

5.2 Effects of Energy Loss

Because of radiation damping, each electron loses energy at a rate depending on its energy (Equation 5.4). Consequently, the energy spectrum will not remain constant. The situation is further complicated by the fact that electrons can lose energy by other processes as well. These loss mechanisms have been discussed by a number of authors (87),(88),(89) and are summarized in Table IX.

In these formulae, n is the density of the medium in cgs units, E the electron energy in ev, V the rate of expansion, r the radius, u the r.m.s. velocity of magnetic clouds, ℓ the dimensions of the magnetic inhomogenieties, and ρ the radiation density. Approximating the logarithmic term by a constant, equation 5.4 can be written

$$\frac{dE}{dt} = a+bE+cE^2 \qquad (5.8)$$

where $b = b_1+b_2+b_3$, and $c = c_1+c_2$ (Table IX). a and c will always be negative representing energy loss, and b will be positive or negative depending on whether the effects of statistical acceleration exceed the losses due to expansion and bremsstrahlung.

Table IX

Process	dE/dT (ev/sec)	
Ionization	$-7.62 \times 10^{-9} n\left[20.1 - 3 \ln(\frac{mc^2}{E})\right]$	
Expansion	$-\frac{V}{r} E$	$=b_1E$
Bremsstrahlung	$-8.0 \times 10^{-16} nE$	$=b_2E$
Fermi Acceleration	$\frac{u^2}{t_c} E$	$=b_3E$
Inverse Compton Effect	$-2.0 \times 10^{-16} \rho c(\frac{E}{mc^2})^2$	$=c_1E^2$
Synchrotron Radiation	$-3.8 \times 10^{-15} H^2E^2$	$=c_2E^2$

Following a procedure outlined by Davis (90), we can determine the effect of these various loss mechanisms on the electron spectrum.

Let all electrons lose energy according to equation 5.8. The number of electrons entering the energy range between E and E=dE is given by

$$\frac{dN_+(E,t)}{dt}dE = N(E+dE,t)\ \frac{d(E+dE)}{dt} + Q(E,t)$$

where $Q(E,t)$ is the rate of injection of relativistic electrons into the system. The number leaving this energy range is then

$$\frac{dN_{-}(E,t)}{dt}\, dE = N(E,t)\, \frac{dE}{dt} \quad .$$

Subtracting, we get

$$\frac{\partial N(E,t)}{\partial t} = \frac{\partial}{\partial E}\left[\frac{dE}{dt} N(E,t)\right] + Q(E,t) \qquad (5.9)$$

giving the fundamental equation governing the time dependence of the electron energy spectrum. Steady state solutions of this equation are given by several authors for certain limiting cases (87),(88), and the time dependent equation has recently been solved by Kardashev (89). We shall seek solutions corresponding to physically plausible conditions and compare these with the observed spectra.

Two special cases will be considered; where there is a monochromatic energy distribution in the injected electrons, and where the injection energy spectrum is given by a power law of the form $Q(E) = KE^{\gamma}$. The latter is the expected spectrum if the electrons are secondaries formed in nuclear collisions of protons having a similar power law spectrum (87).

Before considering the more difficult time dependent equation, we shall look at the limiting equilibrium solutions where $\frac{\partial}{\partial t} N(E,t) = 0$. If the effects of energy loss are

first assumed small, that is a=b=c=0, then from equation 5.9 the electron energy spectrum N(E) is of the same form as the injection spectrum Q(E).

The simplest case is where all electrons are injected into the system with the same energy, E_o at a rate R per unit time. Then from equation 5.9 after a time, T,

$$N(E) = RT\delta\ (E-E_o) \quad ;$$

and, using 5.7, we get

$$P(\nu,\theta) \propto H_\perp \frac{\nu}{\nu_c} F(\frac{\nu}{\nu_c}) \tag{5.10}$$

for the radiation spectrum. As shown in Figure 9, the spectrum is peaked at the value of $\nu \sim .3\nu_c$. Equation 5.10 becomes

$$P(\nu) \approx 5.04 \times 10^{-22} H_\perp (\frac{\nu}{\nu_c})^{1/3} \qquad \nu/\nu_c < .01 \tag{5.11}$$

$$P(\nu) \approx 2.94 \times 10^{-22} H_\perp (\frac{\nu}{\nu_c})^{1/2} e^{-\nu/\nu_c} \qquad \nu/\nu_c > 10 \ . \tag{5.12}$$

As the radiation is highly directed along the direction of the velocity vector, the observer will detect radiation only when the motion of the electron is along the line of sight between the observer and the electron. The angle θ can then be interpreted as the angle between the line of sight and the direction of the magnetic field.

If the distribution of electron energies is given by

$$N(E) = \begin{cases} KE^{\gamma} & E_1 < E < E_2 \\ 0 & E < E_1, E > E_2 \end{cases} \tag{5.13}$$

then equation 5.9 becomes*

$$P(\nu,\theta)=\frac{1}{2}CKL^{-\frac{1}{2}(\gamma+1)}H^{\frac{1}{2}(\gamma-1)}(\mathrm{Sin}\theta)^{\frac{1}{2}(\gamma-1)}\int_{\xi_2}^{\xi_1}\xi^{-\frac{1}{2}(\gamma+3)}F(\xi)d\xi. \quad (5.14)$$

For most values of γ the major contribution to the integral in 5.14 occurs when ξ is of the order of unity. Thus the integral is essentially constant for all values of ν well away from the frequencies corresponding to E_1 and E_2, and we can extend the limits from zero to infinity. Equation 5.14 then becomes

$$P(\nu) \propto \nu^{(\gamma+1)/2} \quad . \quad (5.15)$$

The error introduced by this procedure depends strongly on the value of γ and for $\gamma\sim 0$ the approximation breaks down completely. However, for most values of γ that occur in practice, equation 5.16 gives a good approximation to the radiation spectrum for frequencies $<.1\nu_2$ and $>3\nu_1$. Comparing this to the observed spectral dependence, we obtain the well known relation

$$\alpha = \frac{1}{2}(\gamma+1) \quad . \quad (5.16)$$

Thus, the spectral index of the radiation α , immediately gives the index of the energy spectrum and is independent of the strengtn of the magnetic field. The fact

---

*In the following, we shall drop the explicit dependence on θ and use H to represent $H\mathrm{Sin}\theta$ suitably averaged over θ .

that the flux density of most sources does indeed exhibit a power law dependence on frequency, implies that the electron energy spectra must be closely represented by a power law of the form $N(E) = KE^{\gamma}$ where $\gamma = 2\alpha-1$. With $\alpha = -0.75$, we have $\gamma = -2.5$. As is well known, this is very close to the spectrum of primary cosmic ray protons within our own galaxy and provides support for the hypothesis that the relativistic electrons are formed as a result of collision between protons and nuclei (cf.87). The extremely narrow spread in the observed spectral indices implies a narrow distribution of the electron spectra suggesting a similar acceleration mechanism among the extragalactic sources.

Equation 5.14 has been numerically integrated for several values of γ using an IBM 7090 computer. The results are shown in Figure 15. Below ν_{1c} the flux density falls off slowly and above ν_{2c} quite rapidly.

Following (88) we now suppose that the electrons lose energy by one or more of the processes in Table IX. Then with $\frac{\partial N(E,t)}{\partial t} = 0$ the general solution to (5.9) is

$$N(E) = \frac{-\int_0^E Q(E)dE}{a+bE+cE^2} \quad . \tag{5.17}$$

Thus, a power law spectrum, $Q(E) = KE^{\gamma}$ gives

$$N(E)\alpha \quad \frac{E^{\gamma+1}}{a+bE+cE^2} \quad . \tag{5.18}$$

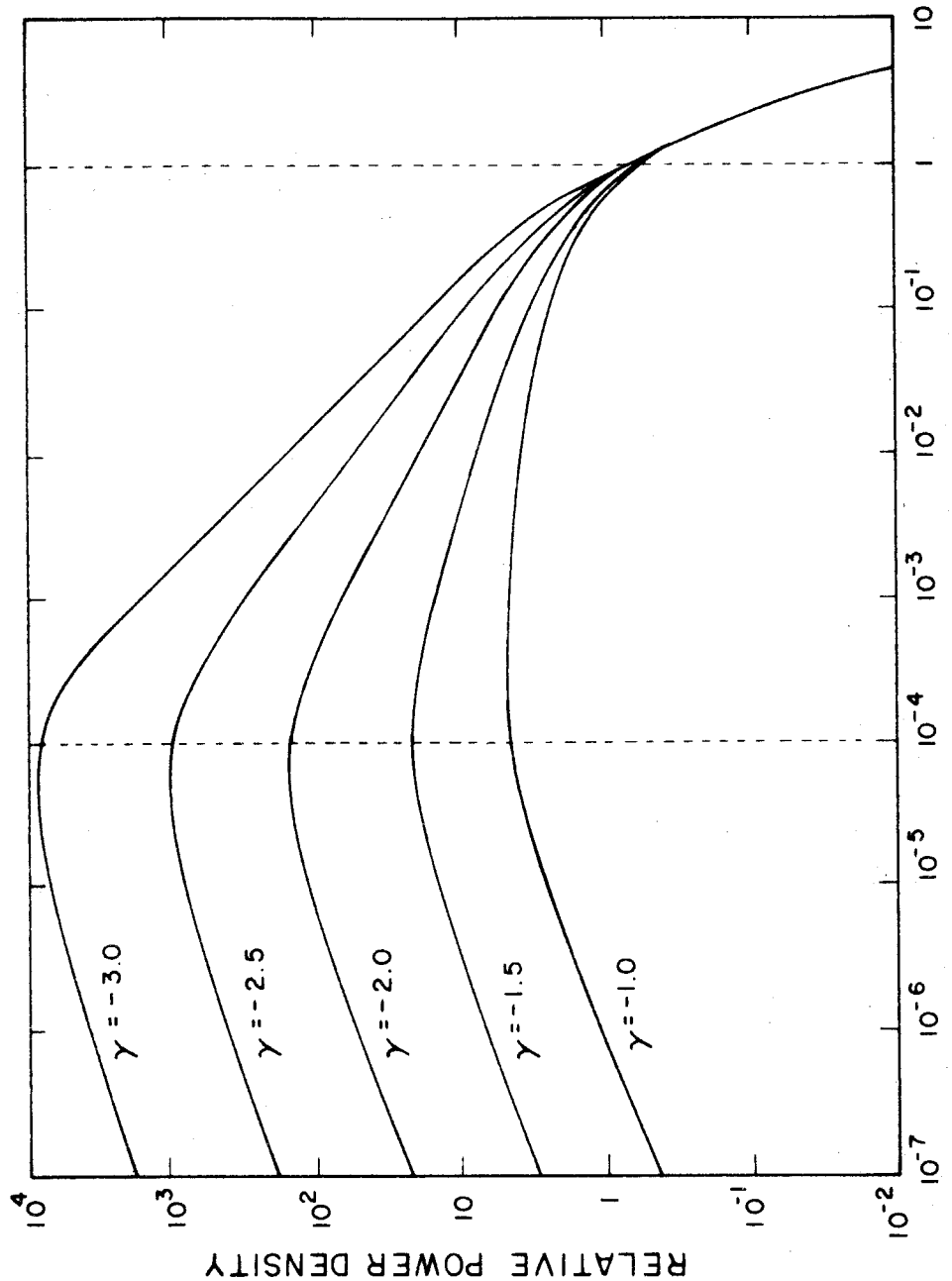

Figure 15 Theoretical radiation spectrum for various values of γ. The dotted lines represent the upper and lower cutoff frequencies.

Table X shows the particular form of the energy and radiation spectrum in regions where the constant, linear, or quadratic terms in the denominator or equation 5.18 dominate. γ_o denotes the index of the injection spectrum and $\alpha_o = (\gamma_o+1)/2$ the corresponding spectral index of the radiation.

Table X

Dominant Loss Mechanisms	Energy Spectrum N(E)	Radiation Spectrum P(ν)
Ionization	E^{γ_o+1}	$\nu^{\alpha_o+1/2}$
Expansion Bremsstrahlung Fermi Acceleration	E^{γ_o}	ν^{α_o}
Inverse Compton Effect Synchrotron Radiation	E^{γ_o-1}	$\nu^{\alpha_o-1/2}$

Thus, at low frequencies the spectral index is flatter by 0.5 than the initial index, at intermediate frequencies the same, and at high frequencies steeper by 0.5. Consequently, near frequencies corresponding to transitions in the dominant loss mechanism (i.e. $cE^2 = bE$, or $a = bE$) we expect to find a "break" in the spectrum with the spectral index changing by 0.5. This is close to the value found in Chapter IV for the curvature index of many of the Class C sources.

In order to expore further the possibility that this mechanism is responsible for the observed curvature of the

spectra, we will consider a special case of equation 5.17 and use equation 5.7 to determine the radiation spectrum. Under conditions expected in extragalactic sources, losses due to ionization and the inverse Compton effect can be neglected (87). Figure 16 shows the radiation spectrum for γ_o=-2.0. The spectrum of an electron distribution with a sharp "break" is also shown for comparison. The energy and frequency scales are of course in arbitrary units; thus the results are applicable for any combination of loss mechanisms and magnetic field strengths. The "break" in the energy spectrum occurs when the effects of expansion, bremsstrahlung, and Fermi acceleration balance the losses due to synchrotron radiation. The frequency of the corresponding break in the radiation spectrum then depends only on the value of the magnetic field and occurs at approximately the critical frequency corresponding to the energy where the losses that are linear in E balance those that are quadratic in E (dotted line in Figure 16).

In figure 16, curve (a) shows that the spectral index changes very slowly with frequency, requiring a range of frequencies of nearly a factor of 100 for the index to change from -1.0 to -0.5. Although this is typical of some of the Class C_H sources, i.e. 3C 338, 3C 438, and 3C 444, it seems unlikely that the effect of different loss mechanisms can explain the curvature of the Class C_L sources where the spectrum changes by $\sim$ 0.5 over a rather small frequency

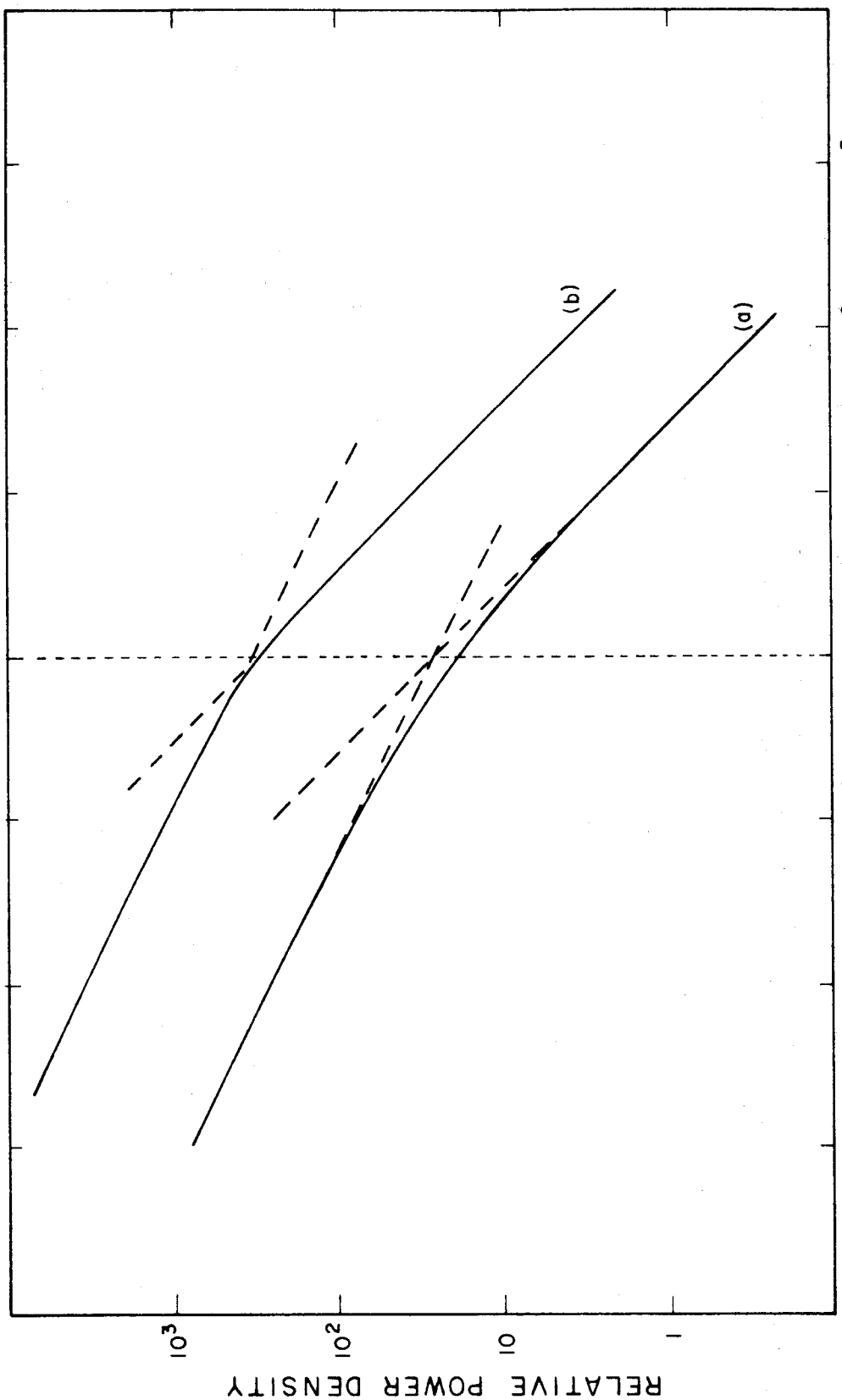

Figure 16 Curve (a) radiation spectrum for $\gamma=-2.0$ in a medium where the electrons are losing energy at a rate proportional to $bE+cE^2$. Dotted line is where $bE=cE^2$. Curve (b) radiation spectrum for sharp "break" in energy spectrum. Dotted line represents the critical frequency corresponding to the "break".

range. This implies a relatively sharp "break" in the energy spectrum as shown by curve (b) in Figure 16.

The typical Class C source has its maximum curvature at about 400 Mc. In a field of 10^{-4} Gauss this corresponds to a "break" in the energy spectrum at about 1 Bev. Due to synchrotron radiation these electrons will lose energy at a rate of about 4×10^{-5} ev/sec, which must be compared with the other possible loss mechanisms.

A density of 500 cm^{-3} is required to produce bremsstrahlung losses of this magnitude. At this density, and with a uniform field of 10^{-4} Gauss, Faraday rotation would produce a rotation of the plane of polarization of about 2×10^{8} radians/$meter^2$. Seilestad has found that the amount of rotation that occurs within the sources themselves is probably less than 25 radians/$meter^2$ (69). Thus the density of electrons must be less than the quantity $10^{9} \langle H_{11} \rangle$, where $\langle H_{11} \rangle$ is the average value of longitudinal component of the magnetic field. Since most sources are observed to be several per cent linearly polarized, it follows that $\langle H_{11} \rangle$ is not likely to be less than a few orders of magnitude below the value of the magnetic field derived from energy considerations. Thus, the density must be less than about .1 cm^{-3} and the effects of bremsstrahlung negligible. Moreover, we note that the corresponding emission measure is less than 300 cm^{-6}-psc, and thus the effects of absorption by free-free transitions of thermal electrons must also be

negligible over the observed radio spectrum.

In order for expansion losses to equal the synchrotron radiation losses, the velocity of expansion would have to be comparable with the speed of light. Furthermore, the rate of expansion would be such that the source attained its present size in a time short compared with the lifetime of an electron and thus our assumption of equilibrium would be violated.

Since nothing is known about the dimensions of the magnetic inhomogenieties, ℓ, or their random velocities, v, it is difficult to determine the effects of statistical acceleration on the distribution of electron energies. However, rough calculations indicate that the conditions necessary for Fermi acceleration to exceed the losses due to synchrotron radiation for 1 Bev electrons are not likely to exist in extragalactic sources.

5.3 Time Variations of the Spectra

Although these arguments are by no means conclusive, it is clear that with the possible exception of the Class C_H sources, there are great difficulties involved in trying to explain the observed form of the spectra if we presume that the spectrum remains constant with time. It is therefore natural to explore the possibility that the Class C sources are very young sources in the process of evolution and that their spectra are changing with time.

Since synchrotron losses will probably dominate the other loss mechanisms, we have $cE^2 >> bE$ and $cE^2 >> a$ in expression 5.8, and equation 5.9 becomes

$$\frac{\partial N(E,t)}{\partial t} = AH^2 \frac{\partial}{\partial E}\left[E^2 N(E,t)\right] + Q(E,t) \quad . \qquad (5.19)$$

Solutions of this equation thus give the energy spectrum as a function of time; equation 5.7 can then be used to find the time dependence of the spectral distribution of the radiation.

The solution to equation 5.19 for various forms of $Q(E,t)$ is quite complex. However, we can get some insight into the behavior of the radiation spectrum as a function of time, by considering the particularly simple case where the electrons are injected into the magnetic field with a monochromatic distribution of energy. With

$$Q(E,t) = \begin{cases} R\delta(E-E_o) & t>t_1 \\ 0 & t<t_1 \end{cases}$$

the solution to 5.19 is (89)

$$N(E,t) = \begin{cases} \dfrac{R}{AH^2E^2} & E_c \le E \le E_o \\ 0 \quad E>E_o\,, \quad E<E_c & \end{cases} \qquad (5.20)$$

where $$E_c = \frac{E_o}{1+AH^2E_o(t-t_1)} \quad .$$

The radiation spectrum as a function of time for such an injection spectrum has been determined by numerical integration of equation 5.7 and is shown in Figure 17. We see from equation 5.20 that for $t \gg 1/AH^2E_o$ we have a power law spectrum of electron energies with $\Upsilon = -2.0$. The corresponding radiation spectral index is then $\alpha = -0.5$.

We shall next consider the case where the electron injection spectrum is a power law of the form

$$Q(E,t) = \begin{cases} KE^{\Upsilon_o} & 0<t<t_1 \\ 0 & t<0, \quad t>t_1 \end{cases} . \qquad (5.21)$$

If we suppose that $t_1 \gg 0$, then at some time t where $0 \ll t \ll t_1$ we can determine the electron energy spectrum in the following way. Using equation 5.6 we can divide the energy spectrum into two regions. At low energies where $E \ll 1/AH^2t$, the electrons will not nave lost a significant amount of energy by radiation and therefore $\Upsilon = \Upsilon_o$. If on the other hand $E \gg 1/AH^2t$, the energy spectrum will be in equilibrium and equation 5.17 is valid giving $\Upsilon = \Upsilon_o - 1$. The frequency corresponding to the separation of the two energy regions is then

$$\nu_b \sim \frac{L}{A^2H^3t^2} \sim \frac{10^3}{H^3t^2} \text{ Mc} . \qquad (5.22)$$

where t is measured in years.

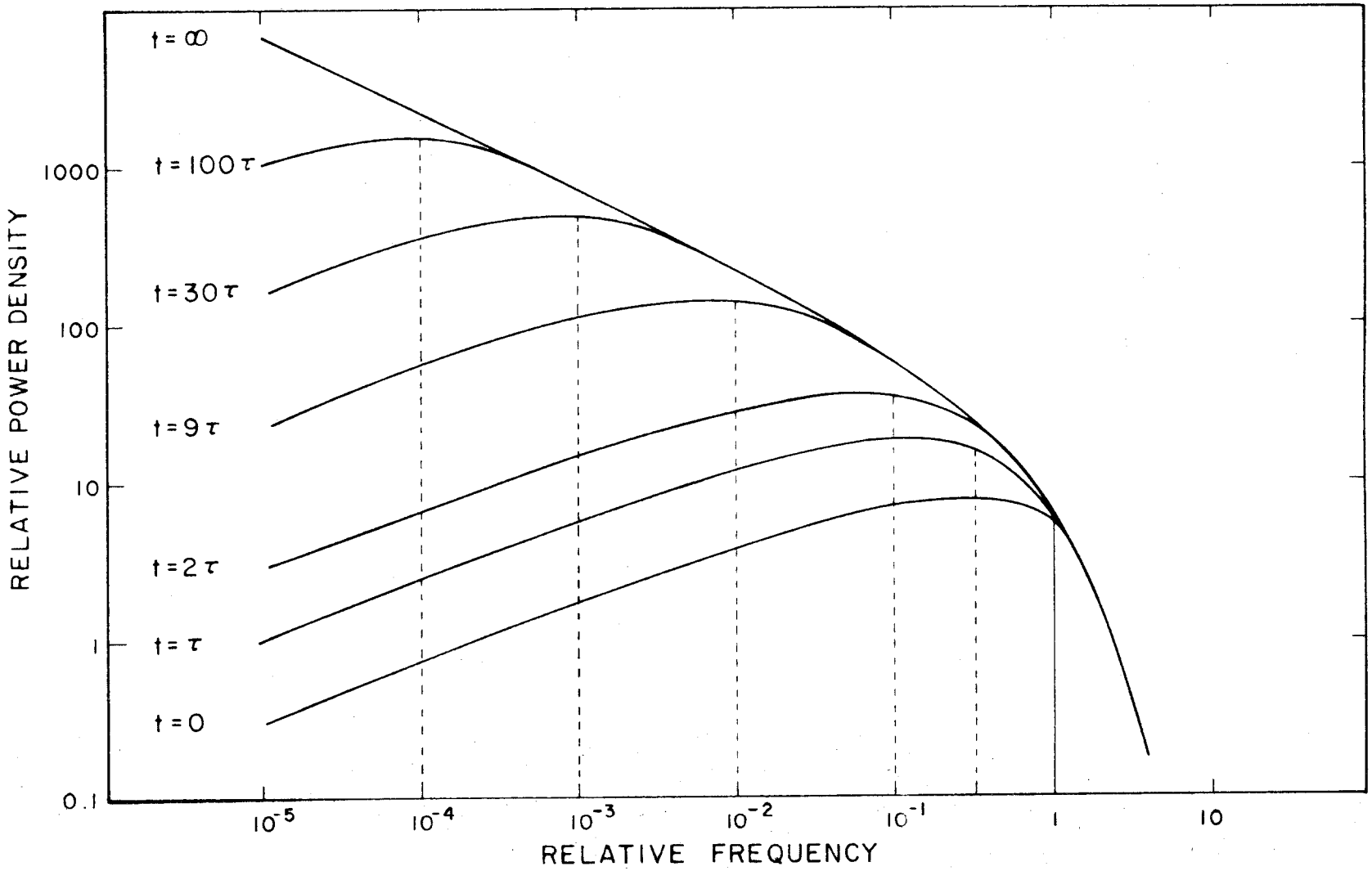

Figure 17 Time dependence of the radiation spectrum when monoenergetic electrons are injected into a uniform magnetic field. The dotted line represents the critical frequency corresponding to the initial electron energy. τ is the characteristic half-life of an electron.

Therefore, to the extent that 5.15 is valid; for $\nu<<\nu_b$, $\alpha = (\gamma_o+1)/2 \equiv \alpha_o$, and for $\nu<<\nu_b$, $\alpha = \gamma_o/2 = \alpha_o = -.5$. Thus we have a break in the radiation spectrum whose frequency is given by equation 5.22 with a change in the spectral index of 0.5. After sufficient time, the frequency of the break will fall below the observable frequency range and the source will have a simple power law spectrum with $\alpha = \alpha_o - .5$.

If at some time, t_1, we shut off the supply of electrons, the spectrum will again undergo time variations. With $Q(E,t) = 0$, the solution of 5.19 is (89).

$$P(\nu) = \begin{cases} H^{-(\gamma-1)/2}\ \nu^{(\gamma+1)/2} & \nu<<\nu_o \\ H^{-2}\ t^{(\gamma-5)/3}\ \nu^{(2\gamma-1)/3} & \nu>>\nu_o \end{cases} .$$

Using similar arguments as above we see that the frequency below which the spectral index remains unchanged is given by equation 5.22 with t replaced by $t-t_1$. Above this frequency the spectrum steepens and the power radiated rapidly decreases with time.

5.4 Summary and Conclusions

We are now in a position to interpret the observational material in terms of the above analysis. It will be convenient to first summarize these results.

The majority of the source have spectra which can be closely approximated by a simple power law at least between 38 and 1420 Mc. The spectral index of these sources

forms a narrow distribution, about a median value of -0.76, with some evidence that the widely spaced doubles have particularly steep spectra. The high surface brightness sources have similar indices at decimeter wavelengths but are considerably flatter at meter wavelengths. In addition, there is a small group of sources that have "normal" spectra at the low frequencies but become quite steep at high frequencies.

These various forms of the observed spectral distribution can be tentatively accounted for by the following evolutionary sequence. At some early stage in the history of a radio source, electrons having a power law distribution of energy are injected into a region containing a strong magnetic field. Initially, these electrons have a relatively flat index with $\gamma_0 \sim -1.5$ corresponding to an index of about $\alpha_0=(\gamma_0+1)/2 \sim -.25$ for the radiation spectrum. If the field and upper energy cutoff are sufficiently high there will be appreciable synchrotron radiation at optical frequencies. Due to the more rapid loss of energy by the high energy electrons, the spectrum will show a "break" about a frequency given by equation 5.22 and above this frequency the spectral index of the radiation will be $\alpha = \gamma_0/2 \sim -0.75$. For an observed frequency of the "break" of several hundred Mc and a field of 10^{-4} Gauss, the corresponding age is about 10^6 years. Examples of sources at this stage of evolution would be 3C 48, 3C 119, MSH 05-36, 3C 147, 3C 286, and 3C 295.

For much younger sources the "break" would be above 3000 Mc and the spectral index would be $\alpha = (\gamma_0+1)/2 \sim -.35$ over the observed frequency range, i.e. 3C 273B and 3C 454.1; while for older sources, the "break" would be well below 100 Mc and the spectral index would be $\alpha = \gamma_0/2 \sim -.75$ over the entire observed range as observed for most of the sources. During this time the source is expanding and the surface brightness, and probably the magnetic field, will be rapidly decreasing.

We note that if the frequency corresponding to the upper cutoff in the electron spectrum is in the observed frequency range, the radiation spectrum will steepen above this frequency. Since we do not necessarily expect a sharp cutoff in the energy spectrum, the radiation spectrum is not likely to steepen as rapidly as shown in Figure 15. The spectra of 3C 338, 3C 438, and 3C 444 show possible evidence of such a partial upper energy cutoff.

Finally, when the supply of relativistic electrons is exhausted, the spectrum will rapidly steepen and for an isotropic distribution of velocities the index will become $\alpha = (\gamma+5)/3 \sim -2$ above a frequency given by equation 5.22. With a field of 10^{-5} Gauss, the steep part of the spectrum will extend below 100 Mc after a time of 10^8 years. For more narrowly confined velocity distributions the spectral index will be even steeper than -2.

As no sources are observed with indices steeper than -1.25, we conclude that the injection of relativistic

electrons must still be continuing, or that all of the observed sources are younger than the characteristic "lifetime" of the most energetic electrons contributing to the observed radiation. In either case, we are faced with the problem of explaining why we do not observe any sources after the electron injection has ceased and the spectrum has begun to decay. If the supply of electrons is continuously replenished, then the source will continue to radiate for many electron "lifetimes" and it seems possible that by the time the reserve electron supply is depleted, the source will have expanded or broken up causing the average surface brightness to be quite low. They would then be difficult to detect - especially with an interferometer.

A number of possible sources with very low average surface brightness have been detected in the 85 Mc survey of Mills, Slee, and Hill (20),(21). It would be interesting to measure the flux density of these sources at decimeter wavelengths to see if their spectra are indeed steep. It is perhaps relevant that the extended low surface sources surrounding M 87 and NGC 1275 do have unusually steep spectra, suggesting that the injection of relativistic electrons into the outer regions of these sources is decreasing with time.

We have of course entirely neglected the difficult questions of the source of relativistic particles and magnetic fields. Although a full discussion of this important problem is beyond the scope of this thesis, we note

that one important result of the present study is that the acceleration mechanism must provide similar energy distributions among sources of vastly different luminosity and spatial extent. If the proposed evolutionary sequence outlined above is correct, then the injection mechanism must specifically provide electrons with an energy density nearly proportional to the minus three halves power of the energy.

REFERENCES

1. G.J. Stanley, O.B. Slee, Australian J. Sci. Research, 3, 234, 1950.

2. G.R. Whitfield, M.N.R.A.S., 117, 680, 1957.

3. G.R. Whitfield, Paris Symposium on Radio Astronomy, R.N. Bracewell, ed., 297, 1959.

4. D.E. Harris, J.A. Roberts, Pub. A.S.P., 72, 237, 1960.

5. D.E. Harris, Ap. J., 135, 661, 1962.

6. R.B. Read, Ap. J., 1963 In press.

7. R.B. Read, I.R.E. Trans. AP-9, 31, 1961.

8. A.T. Moffet, Ap. J. Supp., 7, 93, 1962.

9. B.Y. Mills, O.B. Slee, Australian J. Phys., 10, 162, 1957.

10. M. Ryle, Paris Symposium on Radio Astronomy, R.N. Bracewell, ed., 475, 1959.

11. T.A. Matthews, Quantum Electronics Symposium, C. Townes, ed., 256, 1960.

12. M. Ryle, R.W. Clarke, M.N.R.A.S., 122, 349, 1961.

13. B.Y. Mills, O.B. Slee, E.R. Hill, Australian J. Phys., 14, 497, 1961.

14. A. Hewish, M.N.R.A.S., 123, 167, 1961.

15. T.A. Matthews, private communication, (1963).

16. B. Elsemore, M. Ryle, P.R.R. Leslie, Mem. R.A.S., 68, 61, 1959.

17. D.O. Edge, J.R. Shakeshaft, W.B. McAdam, J.E. Baldwin, and S. Archer, Mem. R.A.S., 68, 37, 1959.

18. A.S. Bennet, Mem. R.A.S., 68, 163, 1963.

19. J.G. Bolton, F. Gardner, M.B. Mackey, private communication, (1962).

20. B.Y. Mills, O.B. Slee, E.R. Hill, Australian J. Phys., 11, 360, 1958.

21. B.Y. Mills, O.B. Slee, E.R. Hill, Australian J. Phys., 13, 672, 1960.

22. P. Maltby, Ap. J. Supp., 7, 124, 1962.

23. L.R. Allen, B. Anderson, R.G. Conway, H.P. Palmer, V.C. Reddish, and B. Rowson, M.N.R.A.S., 124, 477, 1962.

24. A.T. Moffet, private communication, (1963).

25. D.S. Heeschen, Ap. J., 133, 322, 1961.

26. D.S. Heeschen, B.L. Meredith, Pub. N.R.A.O., 1, 121, 1961.

27. J. Högbom, J. Shakeshaft, Nature, 189, 561, 1961.

28. D.S. Heeschen, B. Meredith, Nature, 190, 705, 1961.

29. D.C. Hogg, J. Apl, Phys., 30, 1417, 1959.

30. G.A. Seielstad, R.W. Wilson, Nature, In press, 1963.

31. G.A. Seielstad, D. Morris, V. Radhakrishnan, Submitted to Ap. J.

32. F. Gardner, J.B. Whiteoak, Nature, 197, 1162, 1963.

33. S. Goldstein, A.J., 67, 171, 1962.

34. R.G. Conway, K.I. Kellermann, R.J. Long, M.N.R.A.S., 125, In press, 1963.

35. M. Davis, private communication, (1962).

36. G. Westerhout, B.A.N. 13, 105, 1956.

37. D.S. Heeschen, Pub. A.S.P., 72, 368, 1960.

38. P.S. Pskovskii, Soviet Astr., 6, 172, 1962.

39. D.S. Heeschen, Pub. N.R.A.O., 1, 129, 1961.

40. R. Minkowski, Ap. J., 132, 908, 1960.

41. T.A. Matthews, M. Schmidt, private communication, (1963).

42. T.A. Matthews, A.R. Sandage, Ap. J., In press, 1963.

43. J.L. Greenstein, T.A. Matthews, Paper presented to the 113th Meeting of the A.A.S., Tucson, Arizona, 1963.

44. B.Y. Mills, A.G. Little, and K.V. Sheridan, Australian J. Phys., 9, 218, 1956.

45. K.I. Kellermann, D.E. Harris, Obs. of the C.I.T. Radio Observatory, No. 7, 1960.

46. A.R. Sandage, Ap. J., 133, 365, 1961.

47. A.R. Sandage, A.J., 66, 53, 1961.

48. P. Maltby, T.A. Matthews, A.T. Moffet, Ap. J., 137, 153, 1963.

49. M. Schmidt, private communication, (1963).

50. R.G. Conway, J. Shakeshaft, G.R. Whitfield, The Observatory, 80, 162, 1960.

51. G.R. Whitfield, M.N.R.A.S., 117, 680, 1957.

52. P.R.R. Leslie, B. Elsemore, The Observatory, 81, 14, 1961.

53. W. Baade, R. Minkowski, Ap. J., 119, 215, 1954.

54. C.R. Lynds, S. Sobieski, Pub. N.R.A.O., 1, 155, 1961.

55. C. Hazard, M.B. Mackey, A.J. Shimmins, Nature, 197, 1037, 1963.

56. A.T. Moffet, A.J., 66, 49, 1961.

57. J.E. Baldwin, F.G. Smith, The Observatory, 76, 141, 1956.

58. B.Y. Mills, Australian J. Phys., 6, 452, 1953.

59. J. Lequeux, Ann 'd Astrophys., 25, 221, 1962.

60. R.C. Bless, Ap. J., 135, 187, 1962.

61. G.R. Burbidge, Ap. J., 124, 416, 1956.

62. I.S. Snklovsky, Astr. Zhur, U.S.S.R., 32, 215, 1955.

63. K.V. Sheridan, Australian J. Phys., 11, 400, 1958.

64. J.V. Hindman, C.M. Wade, Australian J. Phys., 12, 258, 1959.

65. J.G. Bolton, B.G. Clark, Pub. A.S.P., 72, 29, 1960.

66. C.A. Shain, C.S. Higgins, Australian J. Phys. 7, 130, 1954.

67. P. Maltby, Nature, 191, 793, 1961.

68. R.N. Bracewell, Stanford Radio Astronomy Institute Publication, No. 15, 1961.

69. G.A. Seielstad, Ph.D. Thesis, California Institute of Technology, 1963.

70. J.H. Oort, T. Walraven, B.A.N., 12, 285, 1956.

71. C.R. O'Dell, Ap. J., 136, 809, 1962.

72. J.B. Oke, Nature, 197, 1040, 1963.

73. H. Walraven, N. Herlofson, Phys. Rev., 78, 616, 1950.

74. K.O. Kiepenheur, Phys. Rev., 79, 738, 1950.

75. J. Shwinger, Phys. Rev., 75, 1912, 1949.

76. V.V. Vladimirski, Zhur. Eksp. Teor. Fiz., 18, 392, 1948.

77. J.L. Greenstein, R. Minkowski, Ap. J., 118, 1, 1953.

78. N. Roman, F.T. Haddock, Ap. J., 124, 35, 1956.

79. J.L. Greenstein, private communication, (1963).

80. R.Q. Twiss, Australian J. Phys., 11, 564, 1958.

81. R.Q. Twiss, Ap. J., 136, 438, 1962.

82. P.F. Browne, Ap. J., 134, 963, 1961.

83. P.F. Browne, Ap. J., 134, 442, 1961.

84. I.S. Shklovsky, Astr. Zhur. U.S.S.R., 29, 418, 1952.

85. V.L. Ginzburg, Dokl. Akad. Nauk U.S.S.R., 76, 377, 1951.

86. K. Westfold, Ap. J., 130, 241, 1959.

87. V.L. Ginzburg, Progress in Elementary Particle and Cosmic Ray Physics, 339, 1958.

88. H. Turner, M.N.R.A.S., 119, 184, 1959.

89. N.S. Kardashev, Soviet Astr., 6, 317, 1962.

90. L. Davis, Phys. Rev., 101, 351, 1956.

91. R.W. Wilson, J.G. Bolton, Pub. A.S.P., 72, 331, 1960.

92. G.C. McVittie, Fact and Theory in Cosmology, 115, 1961.